NBSIR 81-2275

1980 Annual Report: Optical Measurements for Interfacial Conduction and Breakdown

R. E. Hebner, Jr., and E. F. Kelley

Electrosystems Division
Center for Electronics and Electrical Engineering
U.S. Department of Commerce
National Bureau of Standards
Washington, DC 20234

J. E. Thompson and T. S. Sudarshan

University of South Carolina

T. B. Jones

Colorado State University

January 1981

Issued May 1981

NBSIR 81-2275

1980 ANNAUL REPORT: OPTICAL MEASUREMENTS FOR INTERFACIAL CONDUCTION AND BREAKDOWN

R. E. Hebner, Jr., and E. F. Kelley

Electrosystems Division
Center for Electronics and Electrical Engineering
U.S. Department of Commerce
National Bureau of Standards
Washington, DC 20234

J. E. Thompson and T. S. Sudarshan

University of South Carolina

T. B. Jones

Colorado State University

January 1981

Issued May 1981

U.S. DEPARTMENT OF COMMERCE, Malcolm Baldrige, *Secretary*

NATIONAL BUREAU OF STANDARDS, Ernest Ambler, *Director*

TABLE OF CONTENTS

TABLE OF CONTENTS (cont.)

Executive Summary

The design of power system apparatus requires proper placement of the solid insulation, which provides mechanical support as well as electrical insulation, to minimize the electrical stress along the solid-liquid or solid-gas interface. In transformers, for example, the design surface stress is an order of magnitude lower than the partial discharge inception stress of either the solid or the liquid component alone.

The development of more compact systems, therefore, requires materials and/or configurations which permit higher surface stresses. The purpose of this work has been to develop techniques to measure the phenomena which lead to electrical breakdown along an interface. The new measurement techniques which have been developed are the electro-optical measurements of electric field distributions. Specifically, systems have been developed to measure the electric field distribution in transformer oil using the Kerr effect and to measure the surface charge accumulation at a gas-solid interface.

The measurements have been supplemented by calculations of the distortion produced by selected interfacial surface charge distributions. The calculations also serve to relate quantitatively the measured distortion of the electric field to the magnitude of the charge which produced the distortion.

Measurements of the field distribution in transformer oil between parallel-plates show little space charge distortion of the electric field for the relatively pure oil used in these studies. To obtain a more complete picture of interfacial phenomena, breakdown locations and voltages were also determined. With relatively pure materials, there was no statistically-significant preference for breakdown in the vicinity of the interface.

At vacuum-solid interfaces, however, interfacial breakdown was observed and surface charging of the interface was measured. As gas is introduced into

the system, the surface charge is removed so that no effect of surface charging was detected at atmospheric pressure. At pressures above atmospheric, there is evidence that surface charging may again become important.

New measuring techniques, therefore, are being developed which provide useful insight into the behavior of composite insulating systems. These techniques are being developed using waveforms and materials which are useful for power system apparatus. It is anticipated that the results of the electrical, optical, and electro-optical measurements will yield a description of interfacial phenomena which will be useful in the design and/or testing of future insulating systems.

1. INTRODUCTION

The objectives of this investigation are to develop apparatus and appropriate procedures for optical measurement of the interfacial electric field distribution and space charge density in materials for electrical power equipment and systems; to understand the interfacial processes in specific insulation systems; and to demonstrate the applicability of the instrumentation and developed procedure in systems involving liquid-solid, gas-solid, and extruded dielectrics. This report will deal only with progress in the studies of liquid-solid and gas-solid interfaces as the work on extruded dielectrics has been completed and reported.

2. RESEARCH PLAN

The design of power system apparatus requires proper placement of the solid insulation, which provides mechanical support as well as electrical insulation, to minimize the electrical stress along the solid-liquid or solid-gas interface. In transformers, for example, the design surface stress is an order of magnitude lower than the partial discharge inception stress of either the solid or the liquid component alone.[1]

The development of more compact systems, therefore, requires materials and/or configurations which permit higher surface stresses. So, it is apparent that techniques are needed to measure the phenomena which lead to electrical breakdown along an interface. The technical literature suggests that at an interface the electric field is enhanced.[2] On the time scales measured and for the materials studied, however, subsequent research suggests that the enhancement is insufficient to yield the presumed reduction in the breakdown.[3]

To provide a definitive description of the prebreakdown process, it is necessary to measure the electric field distribution. Probes are unsuitable for such measurements because of their poor spatial and temporal resolution and because of the difficulties in developing a probe which does not perturb the system under test. Optical measurement techniques based on the Kerr effect and those based on the Pockels effect however, are suitable for the measurement of interfacial fields.

It is necessary to correlate the electric field measurement with breakdown or, perhaps more importantly, with prebreakdown phenomena at the interface. The correlation requires accurate current and voltage measurements before and during breakdown. It further requires that the location of the breakdown and prebreakdown events be determined.

The results of the electrical, optical, and electro-optical measurements yield a description of the interfacial phenomena which is anticipated will be useful in the design and/or testing of future insulating systems.

To insure that the measurement techniques are useful for power system apparatus, the development was focused on two types of interfaces. One was an oil-solid interface and the other was a compressed gas-solid interface. Recognizing that the specific properties of the insulating material may have an impact on both the measurement technique and the interfacial behavior, these two investigations were pursued in parallel. The specific outputs of both are summarized in the following sections.

3. CALCULATION OF THE ELECTRIC FIELD DISTRIBUTION DUE TO SURFACE CHARGE ON AN INTERFACE PARALLEL TO THE APPLIED FIELD

3.1 Introduction

An optical measurement technique is used to measure insulator surface electric fields as flashover is approached. The physical processes leading to flashover may, however, depend on the temporal and spatial behavior of interfacial surface charge. Analyses have, therefore, been performed to determine the relationship between measured fields and existing surface charge. The stated problem is to determine the surface charge distribution which produces the measured surface electric fields. Electro-optical techniques generally measure the magnitude of the components of the electric field which are perpendicular to the light beam (x-axis):

$$E^2 = E_y^2 + E_z^2 \ . \tag{1}$$

If the direction of the electric field were such that the components E_y and E_z could be determined, then any space charge (or surface charge) could be calculated via Poisson's equation

$$\vec{\nabla} \cdot \vec{E} = \rho / \varepsilon \ . \tag{2}$$

Assuming a surface charge, the field and the resulting electro-optical pattern may be calculated. When the calculated interaction pattern reproduces the experimentally observed pattern then the assumed surface charge distribution is a reasonable approximation to the surface charge produced in the experiment. It is, therefore, necessary to develop methods of field determination from surface charge distributions.

3.2 Laplace's Equation

The geometry relevant to the experimental measurements and the on-going analyses is shown in Fig. 1. It shows two plane electrodes, one located at $(y,z) = (y,0)$ and the other at (y,d). Two insulators, one with permittivity ε_1 and the other with permittivity ε_2, are shown. The interface between these two materials is located in the $y=0$ plane. It is assumed that the material with permittivity, ε_2, extends to $y=\infty$ and that the other extends to $y=-\infty$. The electrodes are assumed to be infinite in extent (x is also a variable). The system extends to $\pm\infty$ in the x direction. The insulators fill the space between the electrodes located at $z=0$ and $z=d$.

Laplace's equation, which determines the potential for the regions bounded by the electrode surfaces and interface shown in Fig. 1, is

$$\nabla^2 \Phi(y,z) = 0 \quad , \tag{3}$$

with the following boundary conditions for the region of interest $(y<0)$:

The potential is defined at both plates

$$\Phi(y,0) = 0 \; , \quad \Phi(y,d) = V \; ; \tag{4}$$

the potential is bounded

$$\Phi(\pm\infty,z) \neq \infty \; ; \tag{5}$$

the tangential field components are continuous across the interface
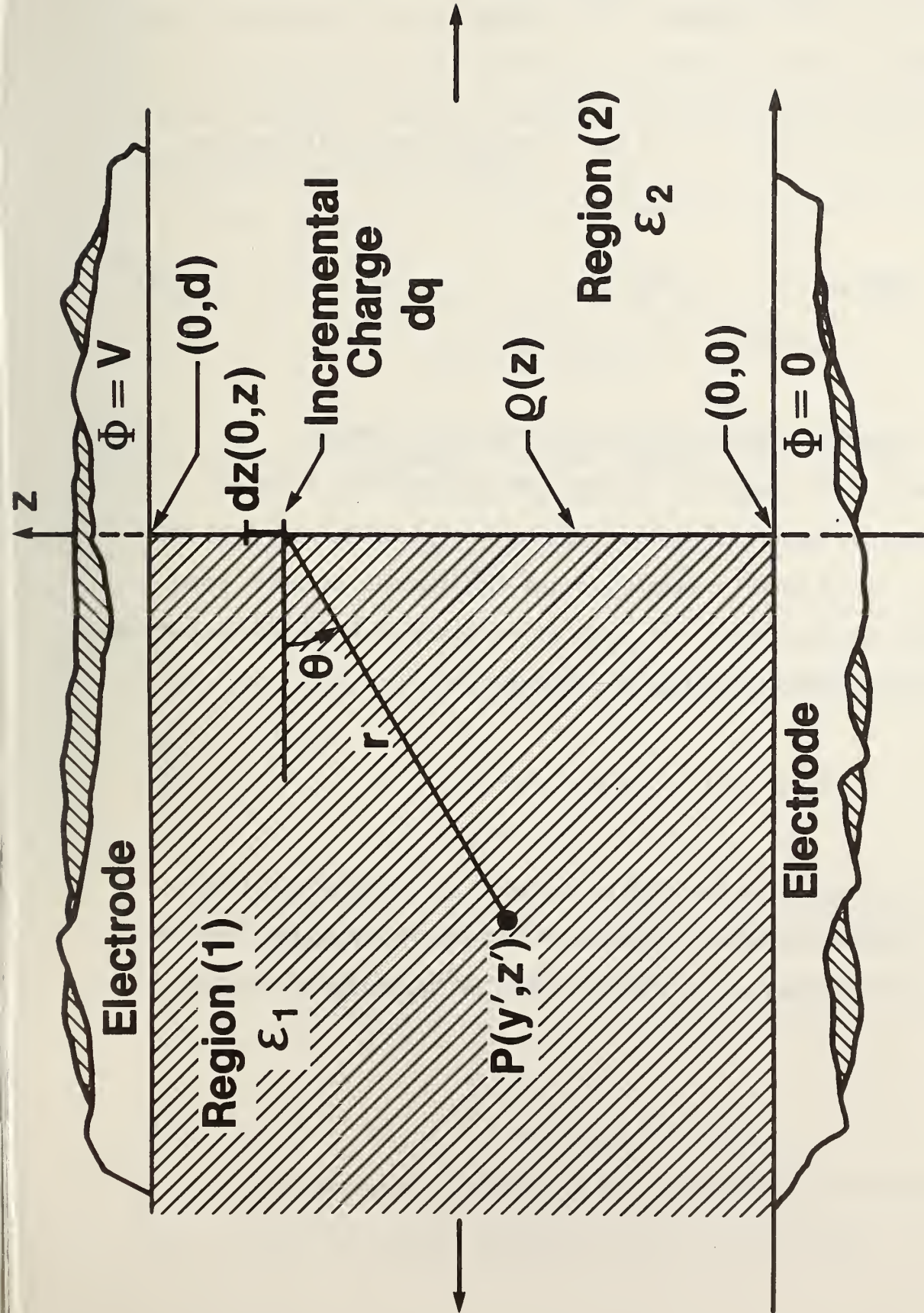
Figure 1. Geometry used in the solution to Laplace's equation.

$$\frac{\partial \Phi(y,z)}{\partial z}\Bigg|_{y=0^+} = \frac{\partial \Phi(y,z)}{\phi z}\Bigg|_{y=0^-} \quad , \tag{6}$$

and there is a discontinuity in the normal component of the displacement vector

$$\varepsilon_1 \frac{\partial \Phi(y,z)}{\partial y}\Bigg|_{y=0^-} - \varepsilon_2 \frac{\partial \Phi(y,z)}{\partial y}\Bigg|_{y=0^+} = \rho(z) \quad , \tag{7}$$

where $\rho(z)$ is surface charge density on the insulator surface.

The last boundary condition deserves some explanation. Given any charged surface, a Gaussian "pill box" may be constructed to show that the discontinuity in the normal component of the displacement vector is equal to the surface charge density. In terms of the electric field and the surface charge of this problem, an equivalent statement is

$$\varepsilon_2 E_{2y}(0^+,z) - \varepsilon_1 E_{1y}(0^-,z) = \rho(z) \quad . \tag{8}$$

This amounts to specifying the normal components of the gradient of the potential along the interface. Equation (6) is simply a statement that the tangential component of the electric field be continuous across the interface:

$$E_{1z}(0^-,z) = E_{2z}(0^+,z) \quad . \tag{9}$$

Thus, the potential is specified on both plates and bounded elsewhere and the first derivatives of the potential are specified along the interface. These are sufficient boundary conditions to determine the potential and field anywhere between the plates.

Laplace's equation is solved by the method of separation of variables where it is assumed that

$$\Phi(y,z) = Y(y)Z(z) \quad .$$

(10)

Since y and z are independent, Laplace's equation requires that

$$\frac{\partial^2 Y}{\partial y^2} = \alpha^2 Y, \qquad \frac{\partial^2 Z}{\partial z^2} = -\alpha^2 Z$$

(11)

where α is an arbitrary constant. For the case of $\alpha=0$ these equations have the solution

$$Y = Ry + S, \quad Z = Pz + Q \quad ,$$

(12)

where R, S, P, and Q are constants. Imposing the boundary conditions, Eqs. (4), (5), and (6) require the solution

$$\Phi_0(y,z) = Vz/d \quad ,$$

(13)

which is the unperturbed potential, i.e., the potential in the case of $\rho=0$. In a similar way, the solution for $\alpha \neq 0$ is found to be

$$\Phi_\alpha(y,z) = (Ae^{i\alpha z} + Be^{-i\alpha z})(Ce^{\alpha y} + De^{-\alpha y}) \quad , \tag{14}$$

or, in terms of trigonometric functions,

$$\Phi_\alpha(y,z) = (A' \cos\alpha z + B' \sin\alpha z)(Ce^{\alpha y} + De^{-\alpha y}) \quad . \tag{15}$$

The boundary conditions, Eqs. (4)-(6), impose the following restrictions on the constants: $\Phi(y,0)=0$ implies $A'=0$; $\Phi(y,d)=V$ for all y implies that $\sin\alpha d=0$ or that

$$\alpha = n\pi/d \quad , \quad n = 1,2,3 \ldots ; \tag{16}$$

$\phi(+\infty,z) \neq \infty$ implies C=0 for $y>0$; $(-\infty,z) \neq \infty$ implies D=0 for $y<0$; and Eq. (6) requires that B'D (for $y>0$) be equal to B'C for ($y<0$) for each n. Calling this last product of constants C_n, the possible potentials for $\alpha\neq0$ are then

$$\Phi_n(y,z) = \begin{cases} C_n \exp(-n\pi y/d)\sin(n\pi z/d), & y>0 \\ C_n \exp(+n\pi y/d)\sin(n\pi z/d), & y<0 \quad . \end{cases} \tag{17}$$

Since any linear combination of solutions is also a solution to Laplace's equation, the general solution for these boundary conditions, Eqs. (4)-(6), is

$$\Phi(y,z) = (Vz/d) + \sum_{n=1}^{\infty} \Phi_n(y,z) \quad . \tag{18}$$

The final boundary condition specifies the normal gradient of the potential

$$\rho_s/(\epsilon_1 + \epsilon_2) = \sum_{n=1}^{\infty} C_n(n\pi/d)\sin(n\pi z/d) \quad . \tag{19}$$

Noting that

$$\int_0^d \sin(n\pi z/d) \sin(m\pi z/d) \, dz = \begin{cases} 0 & \text{for } n \neq m \\ d/2 & \text{for } n = m \end{cases}, \tag{20}$$

the constants C_n may be determined from the surface charge density

$$C_n = [2/n\pi(\epsilon_1 + \epsilon_2)] \int_0^d \rho_s(z)\sin(n\pi z/d) \, dz \quad . \tag{21}$$

This completes the determination of the potential in terms of the surface charge density on the interface. The electric field is then given by

$$\vec{E} = -\vec{\nabla} \Phi \quad . \tag{22}$$

For the above potential, the components of the electric field are

$$E_z = -(V/d) - \sum_{n=1}^{\infty} (n\pi/d) C_n \exp(n\pi y/d) \cos(n\pi z/d) \quad , \tag{23}$$

and

$$E_y = - \sum_{n=1}^{\infty} (n\pi/d) \; C_n \; \exp(n\pi y/d) \; \sin(n\pi z/d) \quad . \tag{24}$$

The magnitude of the field is calculated in terms of these components.

To illustrate the effects upon the field of surface charge distributions, the selected distributions in Fig. 2 are used to determine the predictions of Eqs. 23 and 24. For the purposes of this calculation, it is assumed that the maximum value of the surface charge ρ_0 is 1×10^{-5} C/m^2, that $\varepsilon_1 = \varepsilon_0$ and that $\varepsilon_2 = 21 \; \varepsilon_0$. The calculated solutions for E_y are shown in Fig. 3 and those for E_z are shown in Fig. 4. The values for E_z are calculated for the applied voltage equal to zero. Equation 23, however, indicates that the effect of the applied voltage is to add a constant to each value of E_z (or, equivalently, offset the vertical scale in Fig. 4). There are, probably, some variations in the calculated distribution which are due to the fact that the series expansions are truncated, but the calculated distributions show the anticipated structure.

Thus, a technique has been developed to predict the electric field distortion resulting from a surface charge at the interface between two dielectrics.

4. EXPERIMENTAL ARRANGEMENTS AND RESULTS

4.1. Electro-Optical Measurements in Transformer Oil

4.1.1. Introduction

This section reports the investigation of space charge distortion of the electric field in commercially-pure transformer oil. The measurements reported are Kerr effect measurements, so the electric field is determined by measuring a change in the optical transmittance properties of the oil. Results are presented from experiments using an impulse waveform as well as from those in which 60-Hz voltage was used.
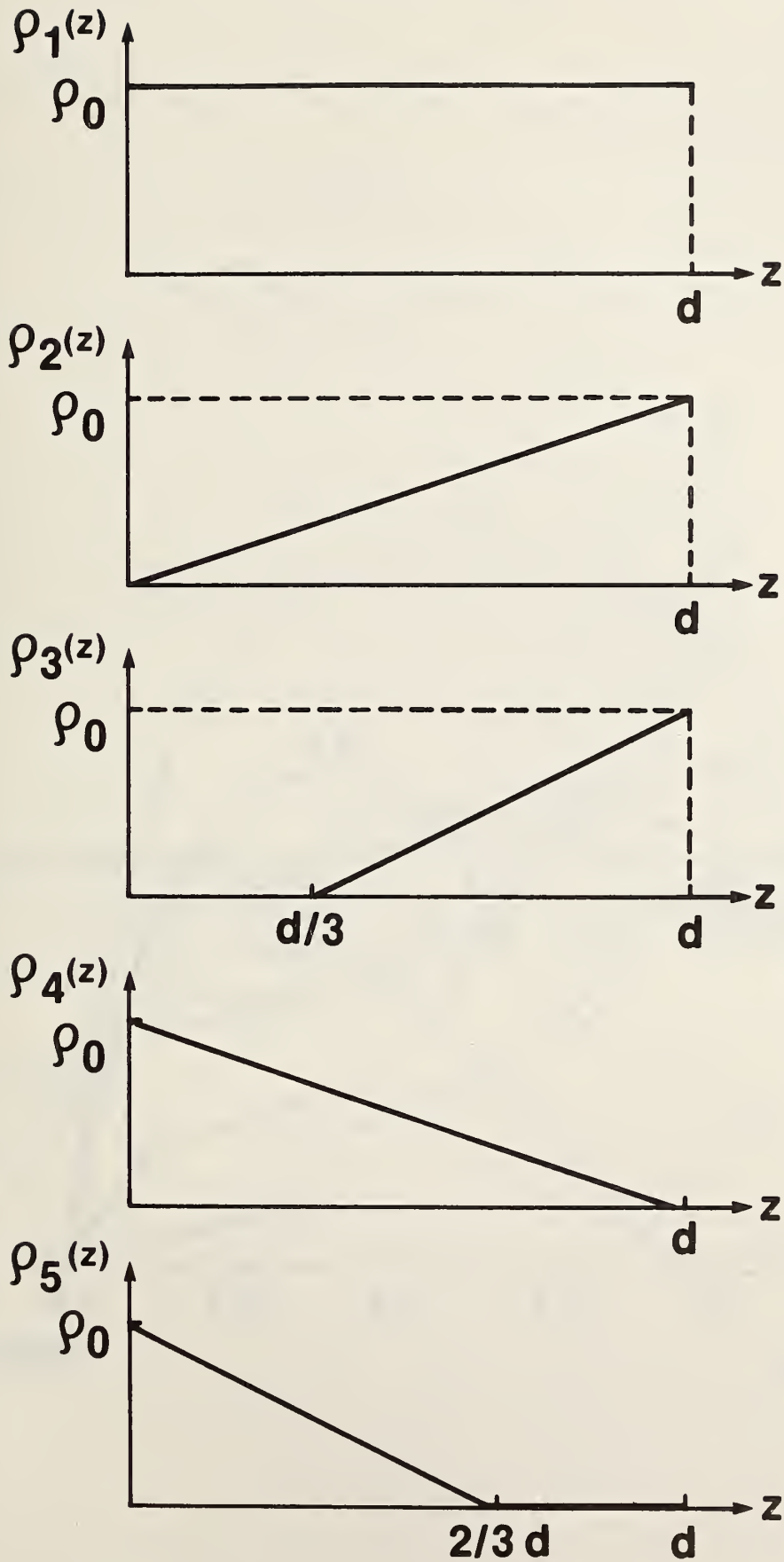
Figure 2.   Assumed surface charge distributions. In the calculations, it was assumed $\rho_0 = 1 \times 10^{-5}$ C/m.
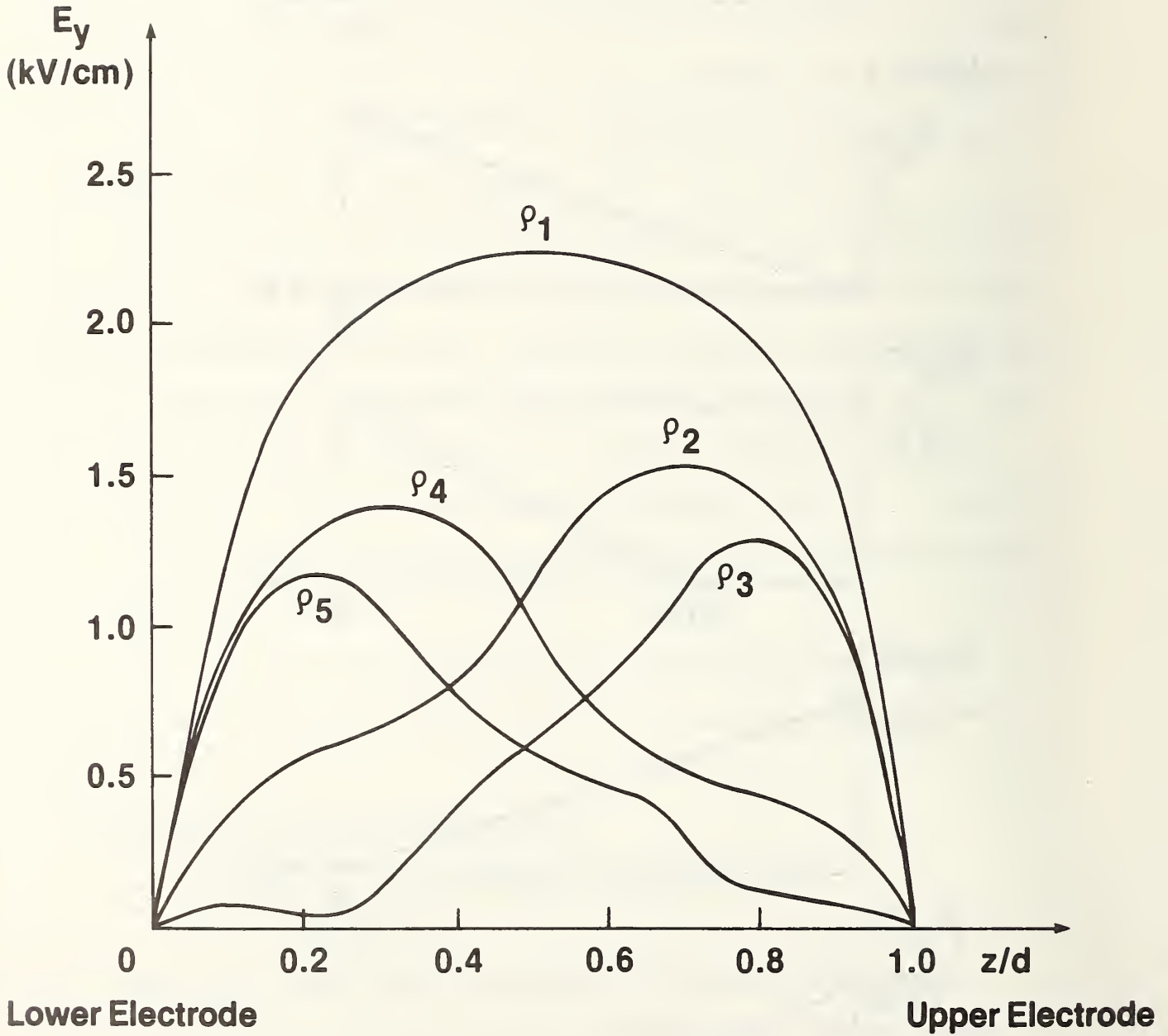
Figure 3.   The calculated electric field component E_y for the surface
charge distributions in Fig. 2
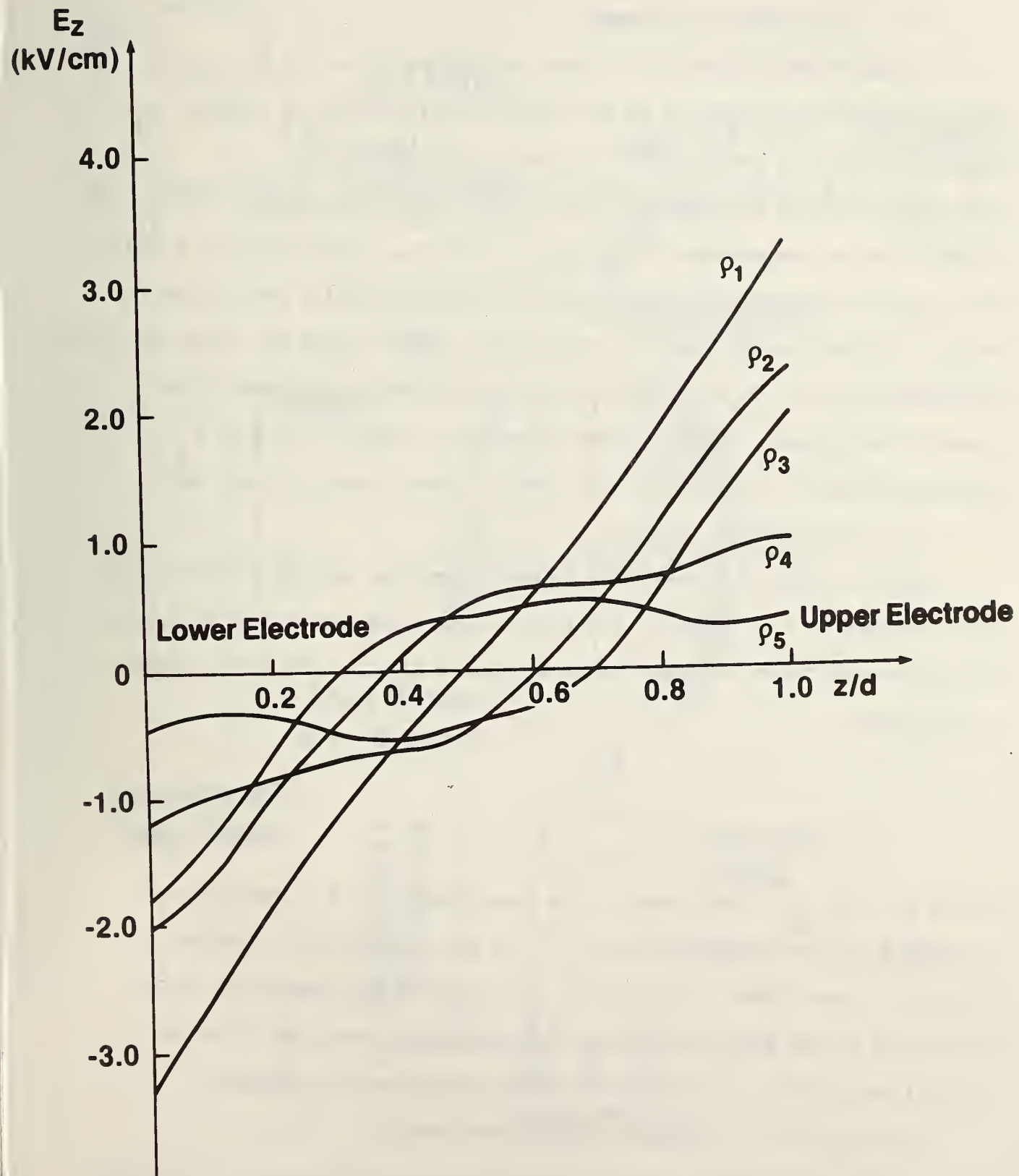
Figure 4. The calculated electric field component E_z for the surface charge distributions in Fig. 2.

4.1.2 Experimental Arrangement

The experimental apparatus is shown schematically in Fig. 5. The
detector permits measurements to be recorded simultaneously at a large
number of points in the y-z plane. Using a pulse generator,
the detector can be activated only for selected intervals of time. For
example, during measurements using impulse voltages, the detector was activated
for 100 ns at the peak of an approximately rectangular pulse with a duration
of 6 μs. Using a 60-Hz waveform, the detector was activated for about 100 ns once
every other cycle. This mode of operation permitted observations to be
made of the average -- over a number of cycles -- electric field at a
preselected point in the cycle, e.g., positive peak, zero crossing, etc.

4.1.3. Experimental Results

Figure 6 shows six Kerr-effect intensity profiles for six different
peak voltages of the impulses. For the parallel-plate test system used, the
maximum transmittance, fringe n=1, occurred near 139 kV. The fringe number
n is given by

$$n = 2BV^2 \ell/d \quad , \tag{25}$$

where B is the Kerr coefficient of the transformer oil, V is the applied
voltage, ℓ is the plate length and d is the plate separation. For the
electrode geometry used (d/ℓ = 0.02), the effect of the geometrical field
distortion at the ends of the electrodes contributes less than 1% to the
optical phase shift. The end field effect, therefore, was ignored.

The Kerr effect is described by the relationship

$$I = I_m \sin^2(\phi/2) \quad , \tag{26}$$

(a)

(b)

$$I(z)=\int_{-w}^{w} I(z,y)dy$$
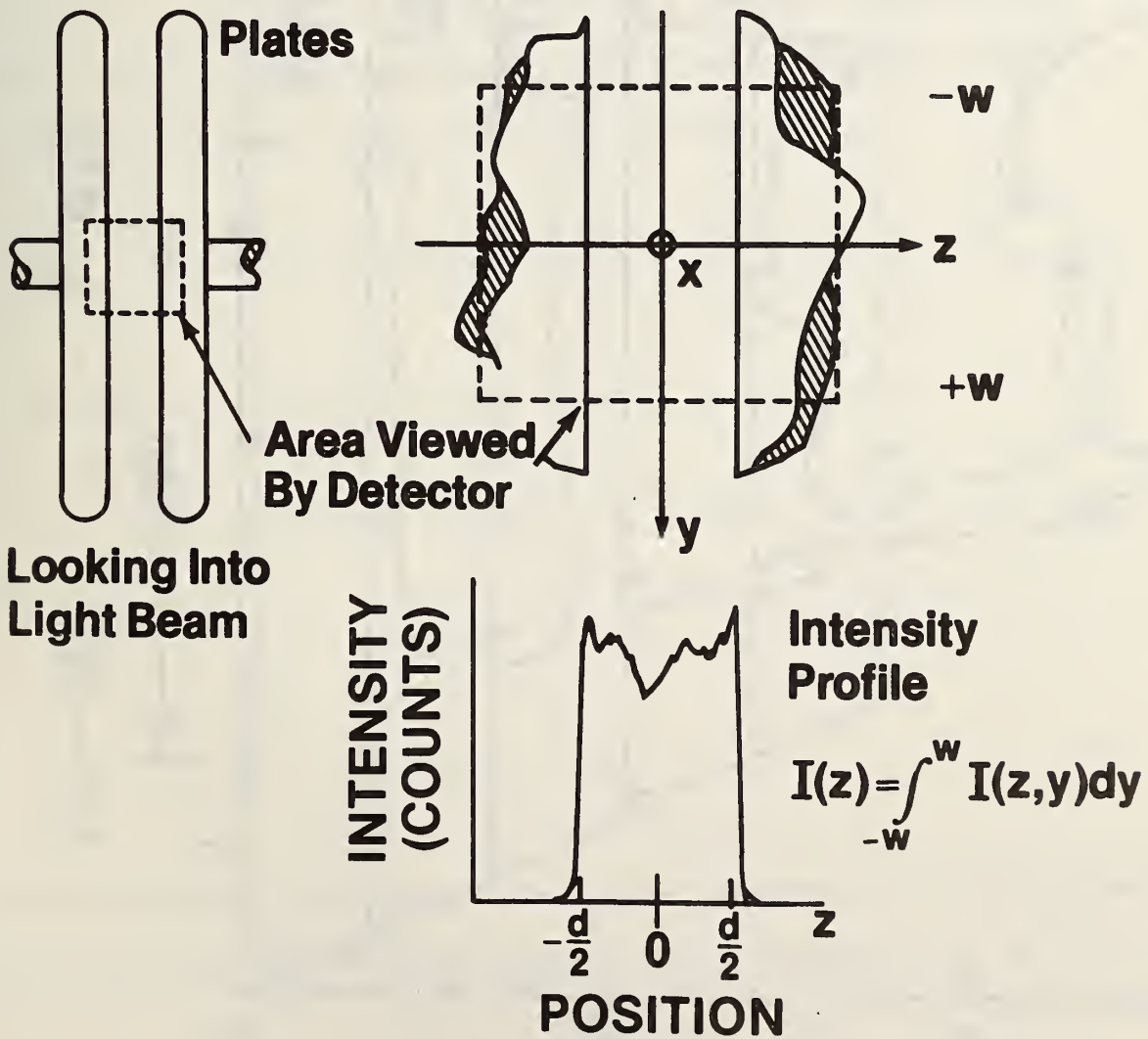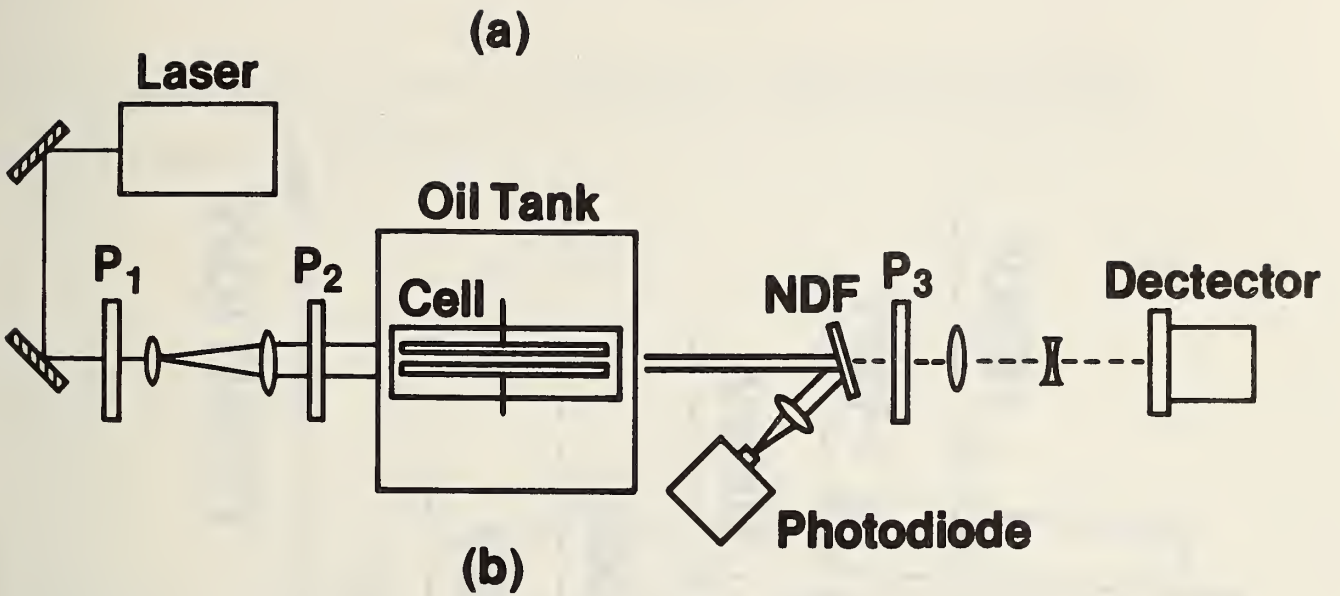
Figure 5. Test arrangement, electrode structure, and typical output data. Polarizers are denoted by P_1, P_2, and P_3 while NDF is a neutral density filter.
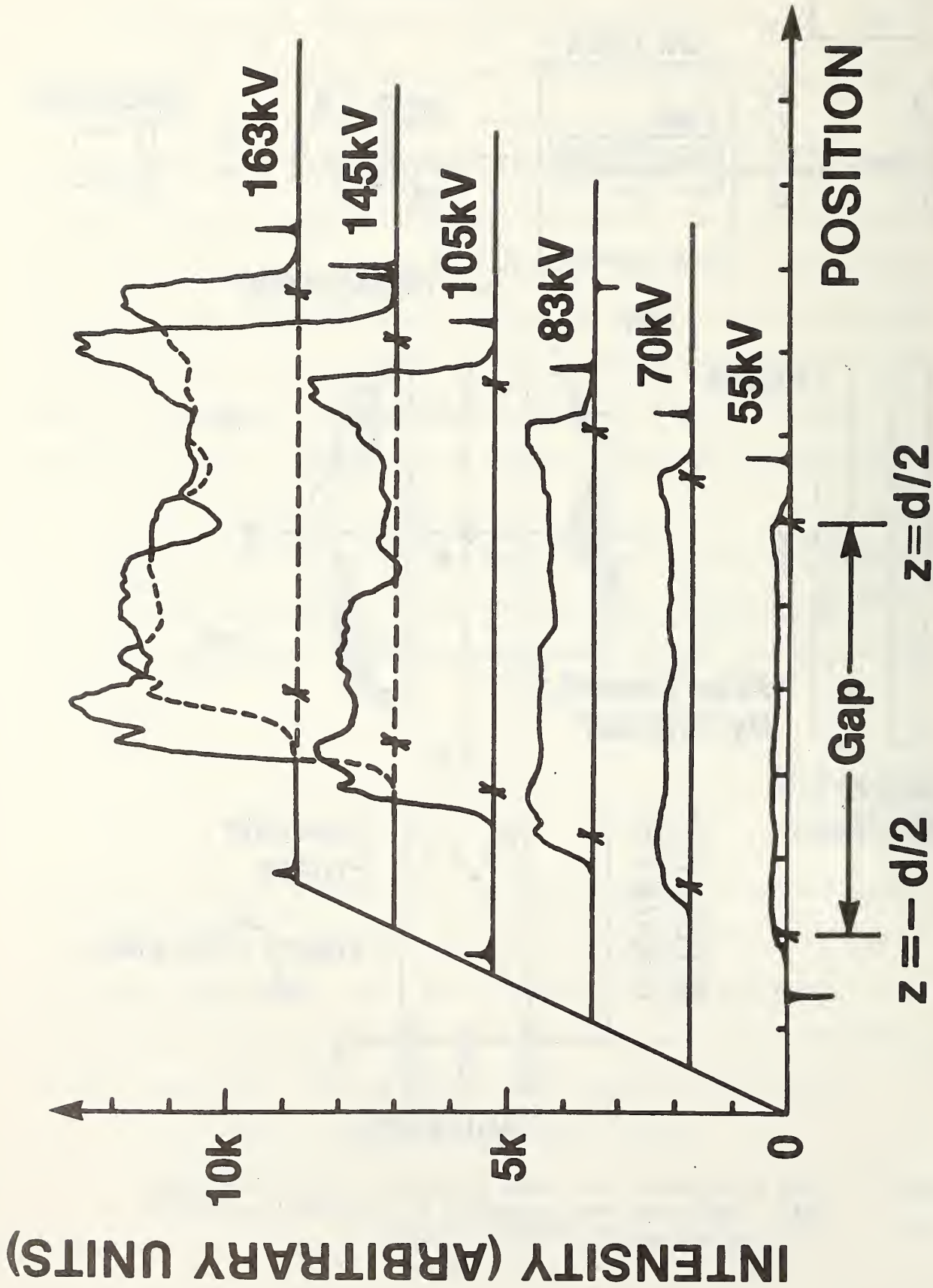
Figure 6. Kerr effect intensity profiles for six different peak impulse voltages.

for crossed polarizers. Here I_m is the maximum transmitted intensity and ϕ is the phase shift given by

$$\phi = 2\pi B \ell V^2/d^2 \quad . \tag{27}$$

From Eqs. 26 and 27,

$$\phi/2 = \sin^{-1}(I/I_m)^{1/2} = (\pi B \ell/d^2)V^2 \quad . \tag{28}$$

A plot of $\sin^{-1}(I/I_m)^{1/2}$ vs. V^2 should yield a straight line with a slope of $\pi B \ell/d^2$. Figure 7 shows such a plot of data taken under impulse voltages. A linear fit (least squares) of the form

$$\sin^{-1}(I/I_m)^{1/2} = \alpha V^2 + \beta \quad , \tag{29}$$

was performed and yielded the values

$$\alpha = (0.0854 \pm 0.0015) \times 10^{-9} \, V^{-2} \quad , \tag{30}$$

and

$$\beta = -0.043 \pm 0.017 \quad . \tag{31}$$

From the value of α and the known experimental parameters (ℓ=0.30m, d=6.4mm), the Kerr coefficient B of the oil used was calculated to be $3.6 \times 10^{-15} m/V^2$.

It should be emphasized that this value may vary among different types of transformer oils and is a function of both oil temperature and the wavelength of the incident light.
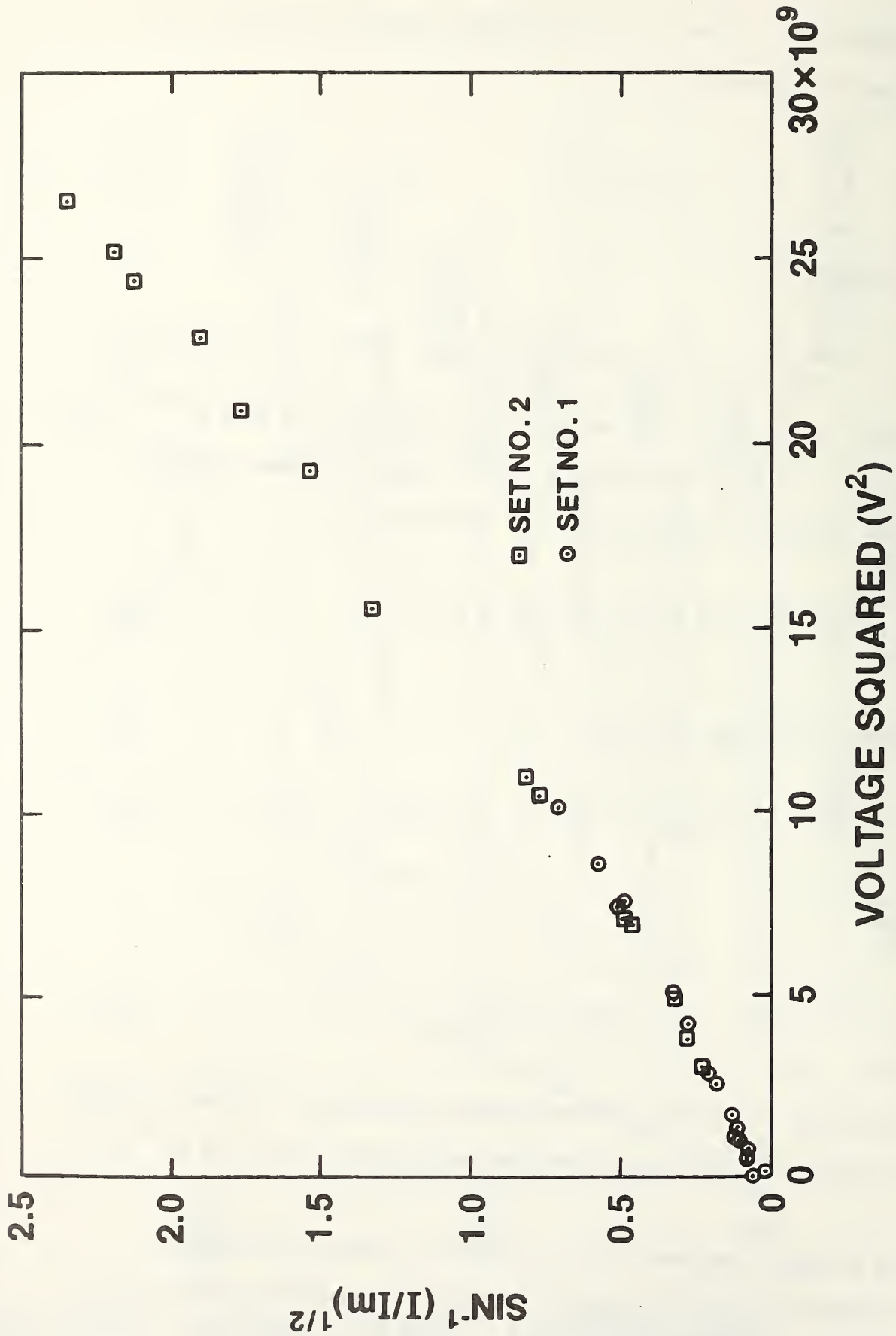
Figure 7. Plot of the voltage squared vs. a function of the measured transmittance yields a straight line as predicted by Eq. 28.

The determination of the Kerr coefficient under impulse excitation demonstrated that the measurement system is capable of recording the electro-optic Kerr effect in transformer oil. The system was then used to measure the electric field distribution under 60 Hz excitation. Figure 9 show two different comparisons of the intensity profile. Figure 8 is a comparison of the shape of the transmittance profile with zero volts applied with the shape of the profile at a positive peak (65.6 kV) of the 60-Hz waveform. If there were significant space-charge distortion of the electric field, then there would be an obvious difference between the two profiles. No such distortion is observed.

A second comparison is shown in Fig. 9. In this case, a 60 kV 60-Hz waveform is applied and the profile is measured at a zero of the voltage waveform. This profile is compared to the light beam profile with no voltage applied. Again, no significant change in shape is apparent. This type of comparison was found to be a good indication of space charge in nitrobenzene[4] because the space charge cannot respond to the instantaneous value of the applied field at 60 Hz, i.e., the space charge distribution remains approximately constant during any cycle of the waveform.

The sensitivity of these measurements can be quantified. Recall the basic relationships for the Kerr effect

$$\phi/2 = \sin^{-1} (I/I_m)^{1/2} = \pi B \ell E^2 \quad . \tag{32}$$

Assume that the electric field can be represented by the sum of the geometric field E_0 and the field caused by space charge E_s, i.e.,

$$E = E_0 + E_s \quad . \tag{33}$$
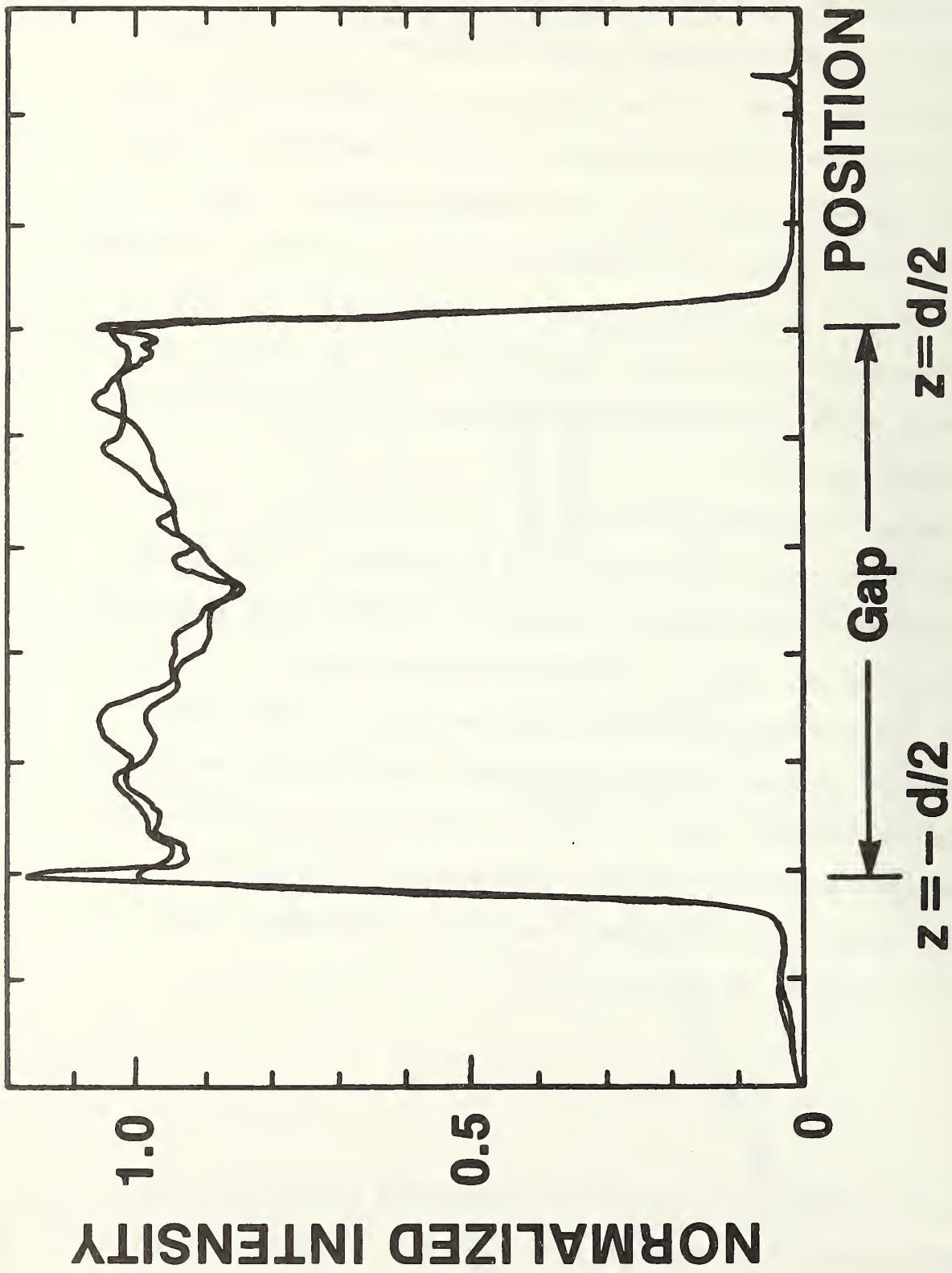
Figure 8.   Comparison of shape of transmittance with 65 kV and with zero volts applied.
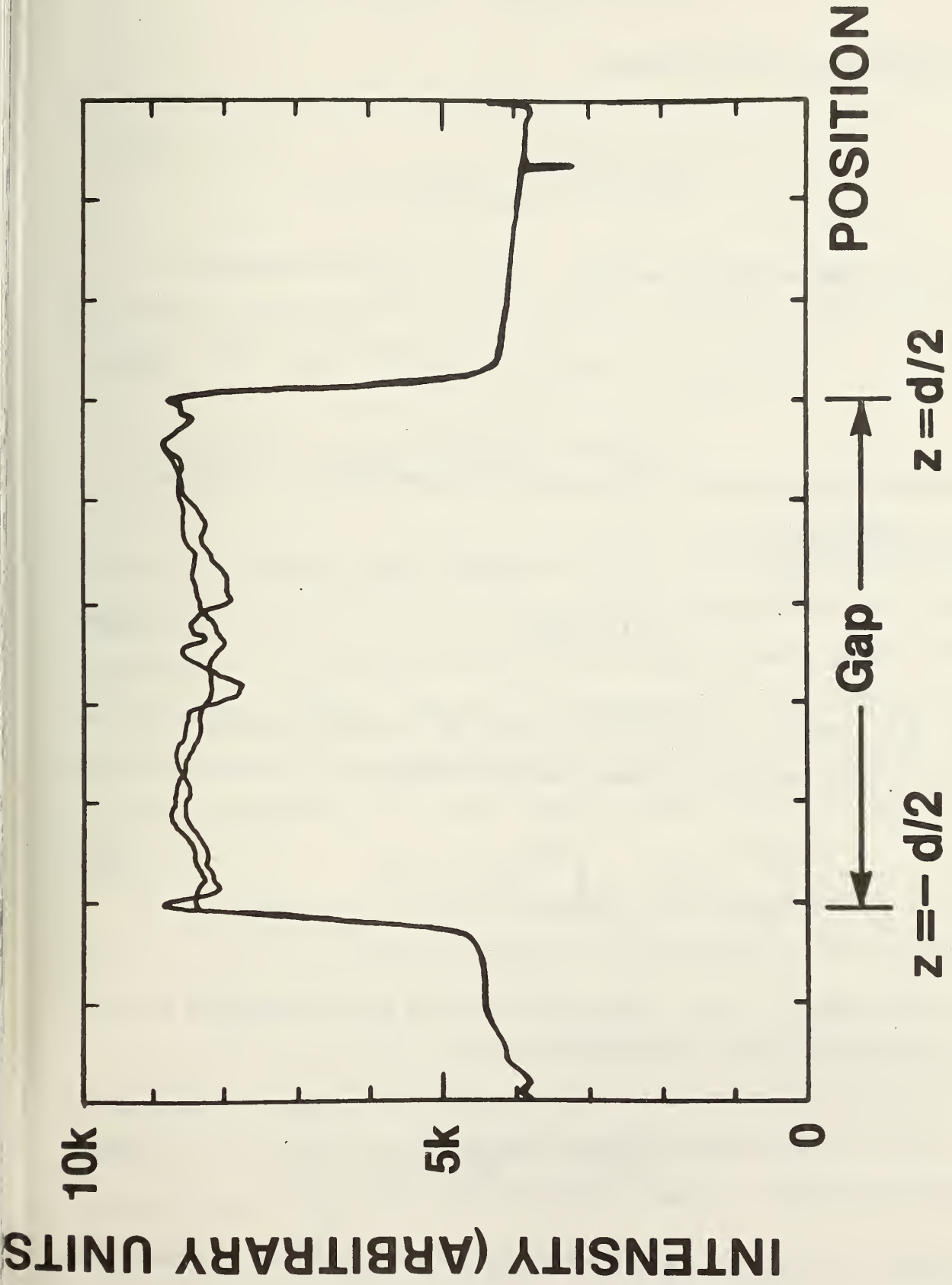
Figure 9.   Intensity with no applied voltage and at a zero crossing of
a 60-Hz wave.

Now, for convenience, we can express

$$E_s = f(z) E_0 \quad , \tag{34}$$

where $f(z)$ is some arbitrary function. Then Eq. 33 can be expressed as

$$E^2 = E_0^2 [1 + 2 f(z) + f^2(z)] \quad . \tag{35}$$

A simple expression for $f(z)$, and one that was appropriate for previous work in nitrobenzene[4] is

$$f(z) = \delta z/_d \quad , \tag{36}$$

where δ is a constant. Note that $f(z)$ cannot be a constant because the path integral of the field must give the voltage, i.e.,

$$V = \int_{-d/2}^{d/2} E \, dz = \int_{-d/2}^{d/2} (E_0 + E_s) \, dz \quad . \tag{37}$$

If we assume that $|E_s| << |E_0|$, then $\delta << 1$, then from Eq. 35 the square of the field can be written approximately as

$$E^2 = E_0^2 (1 + 2\delta z/_d) \quad . \tag{38}$$

As a result, the shape of the intensity profile should exhibit a z- dependence, (Eq. 32),

$$\sin^{-1} (I/I_m)^{1/2} = \pi B \ell E_0^2 (1 + 2\delta z/_d) \quad , \tag{39}$$

or

$$I/I_m = \sin^2 [\pi B \ell E_0^2 (1 + 2\delta z/_d)] \quad . \tag{40}$$

For the 60-Hz data presented in this section, the argument of the sine function is small ($I \lesssim 0.1\ I_m$), so that

$$I/I_m \simeq \pi^2 B^2 \ell^2 E_0^4 (1 + 4\delta z/_d) \quad . \tag{41}$$

This equation indicates that the presence of the assumed space charge distribution changes the slope of the intensity profile by 4δ. This implies, for example, that a 5% change in the field due to space charge distortion would yield a 20% change in the profile. In Figs. 8 and 9, it is estimated that a 10% difference in amplitude between the two intensity profiles would be easily discernable. It is, therefore, concluded that the field distortions due to space charge are less than 2.5%.

As an example, Fig. 10 explicitly shows the relative electric field as a function of position between the plates. In these plots, it can be seen that the electric field is not distorted.

It should also be noted that the application of 60-Hz voltage to transformer oil causes fluid motion and associated optical scattering. Electrical and optical techniques were developed to compensate for this scattering and Fig. 11 shows that negligible changes in the profile occur during a five-minute run.
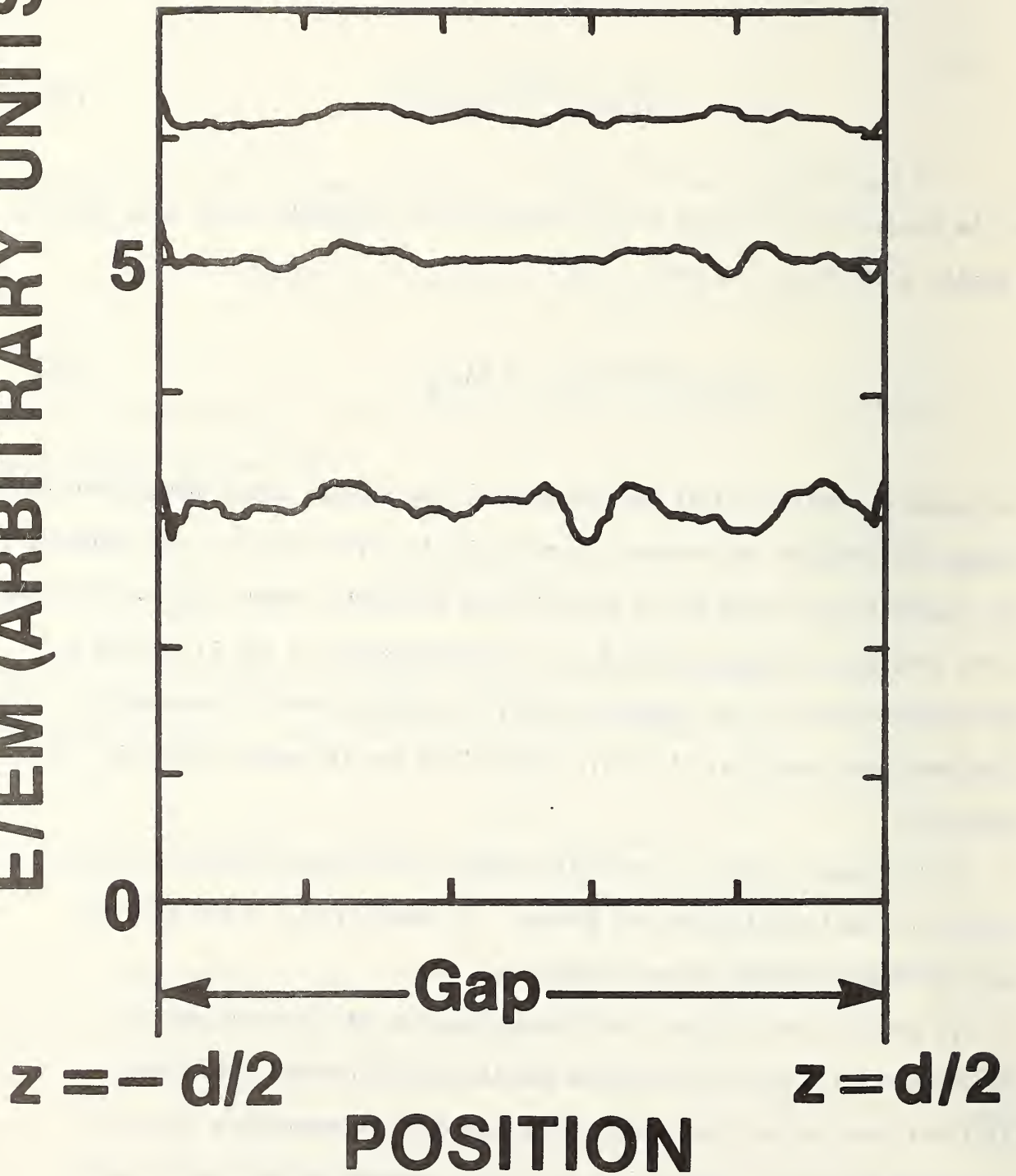
Figure 10.   Relative electric field as a function of position for three
different 60-Hz voltage levels.
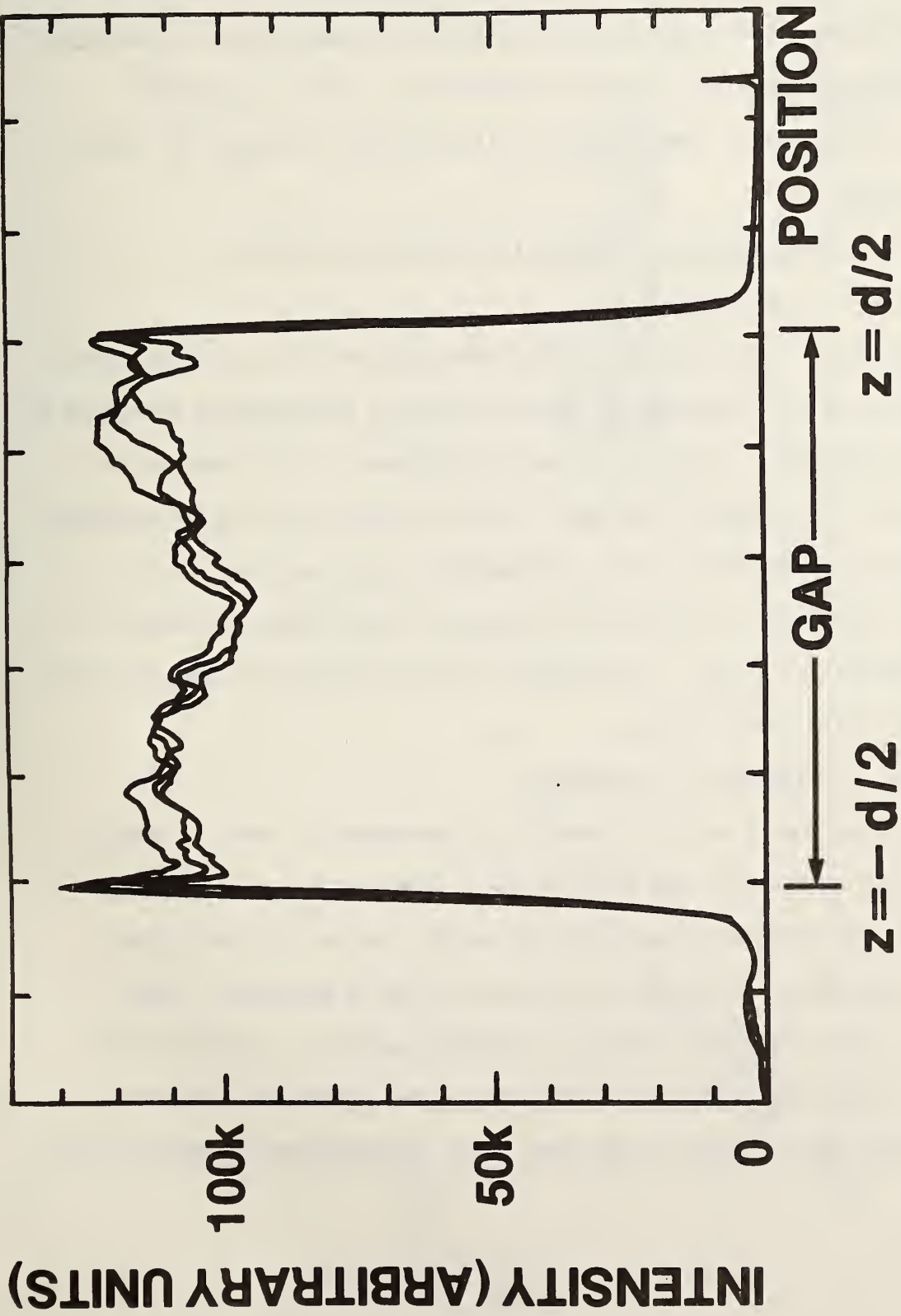
Figure 11. Repeated measurements at the same voltage during a 5-minute test.

Finally, Fig. 12 compares data taken under ac and under impulse waveforms. The ac data yield a Kerr coefficient of 3.1×10^{-15} m/V^2 compared to the value obtained under impulse of 3.6×10^{-15} m/V^2. The differences are somewhat larger than expected and may be due to temperature differences, to a frequency dependence in the Kerr coefficient, or to a systematic difficulty in detection. Measurements will be made to identify the cause of this discrepancy.

4.2. Breakdown Location in Composite Insulating Systems

4.2.1. Introduction

The purpose of this portion of the investigation is to provide a more comprehensive and more fundamental understanding of prebreakdown phenomena at an oil-paper interface. Because of particular concern with power system apparatus, the investigation has been limited to 60-Hz and impulse waveforms.

A significant feature of the experimental program was the use of photographic techniques to record the location of the breakdown event in a composite insulating system. Different electrode shapes were used to obtain a variety of field distributions.

4.2.2. Theoretical Background

Much of the modern work on interfacial breakdown has been influenced by the results of Wechsler and Riccitiello.[2] Their work was apparently motivated by the revision of an American Society for Testing Materials standard test method for dielectric strength of solid materials. They found, under 60-Hz voltages, that the breakdown generally occurred in the liquid at or near the liquid-solid interface. The breakdown strength of the combination was as much as 50% lower than the breakdown strength of the oil alone.
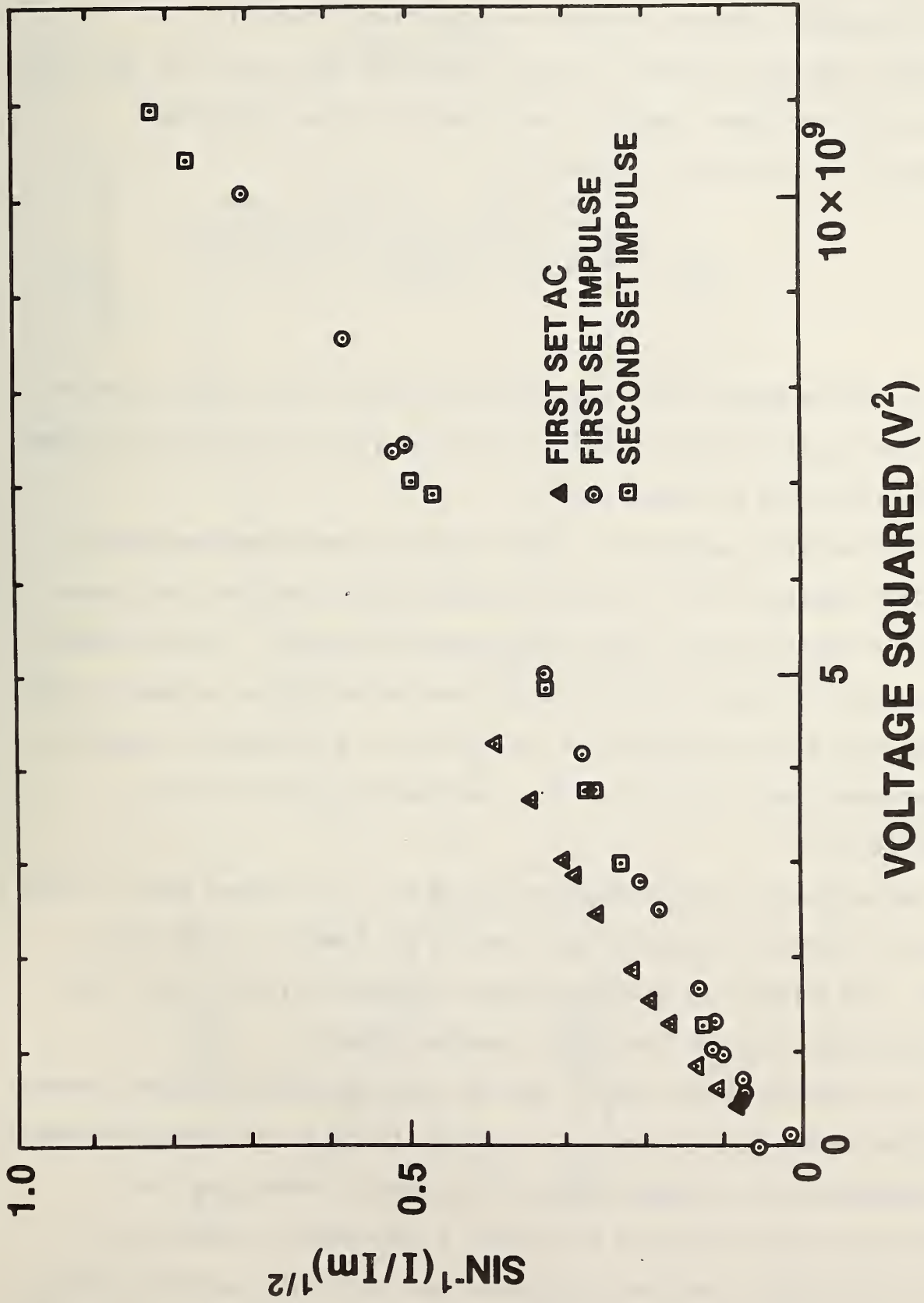
Figure 12. Comparison of 60-Hz and impulse measurements.

To explain these results, they proposed that the breakdown was due to field enhancement caused by surface irregularities on the solid. An idealized interfacial surface is shown in Fig. 13. They calculated that the ratio of the breakdown strength of the composite system to breakdown strength of the fluid alone is given by

$$V_B/V_B' = (1 + \varepsilon_i) \cdot \sum_j z_{sj}/d \quad , \tag{42}$$

where ε_i is the ratio of the relative permittivity of the liquid to that of the solid, z_{sj} is a length element in the solid along the interface (as shown in Fig. 13), and d is the gap spacing.

An alternative explanation of the interfacial breakdown phenomena has also been proposed.[3,5,6] This model attributes the reduction of breakdown voltage at the interface to electrohydrodynamic phenomena. The experimental results which motivated this explanation were Kerr-effect measurements of the steady-state field distribution in the vicinity of a liquid-solid interface, current measurement in the vicinity of the interface, and fluid flow measurements.

Measurements of the steady-state dc electric field showed that the field near the interface differed by approximately 10% from the uniform field value. The authors concluded that these steady-state distributions offer little insight into the interfacial breakdown process.

The measured current density near the interface was significantly greater than the current density through the bulk of the fluid. Separate measurements were performed which suggested that the increase in current was due to electrohydrodynamic motion of the fluid. A subsequent re-examination of this work indicated that the magnitude of the interfacial current is strongly dependent on the geometry of the electrode structure.[7]
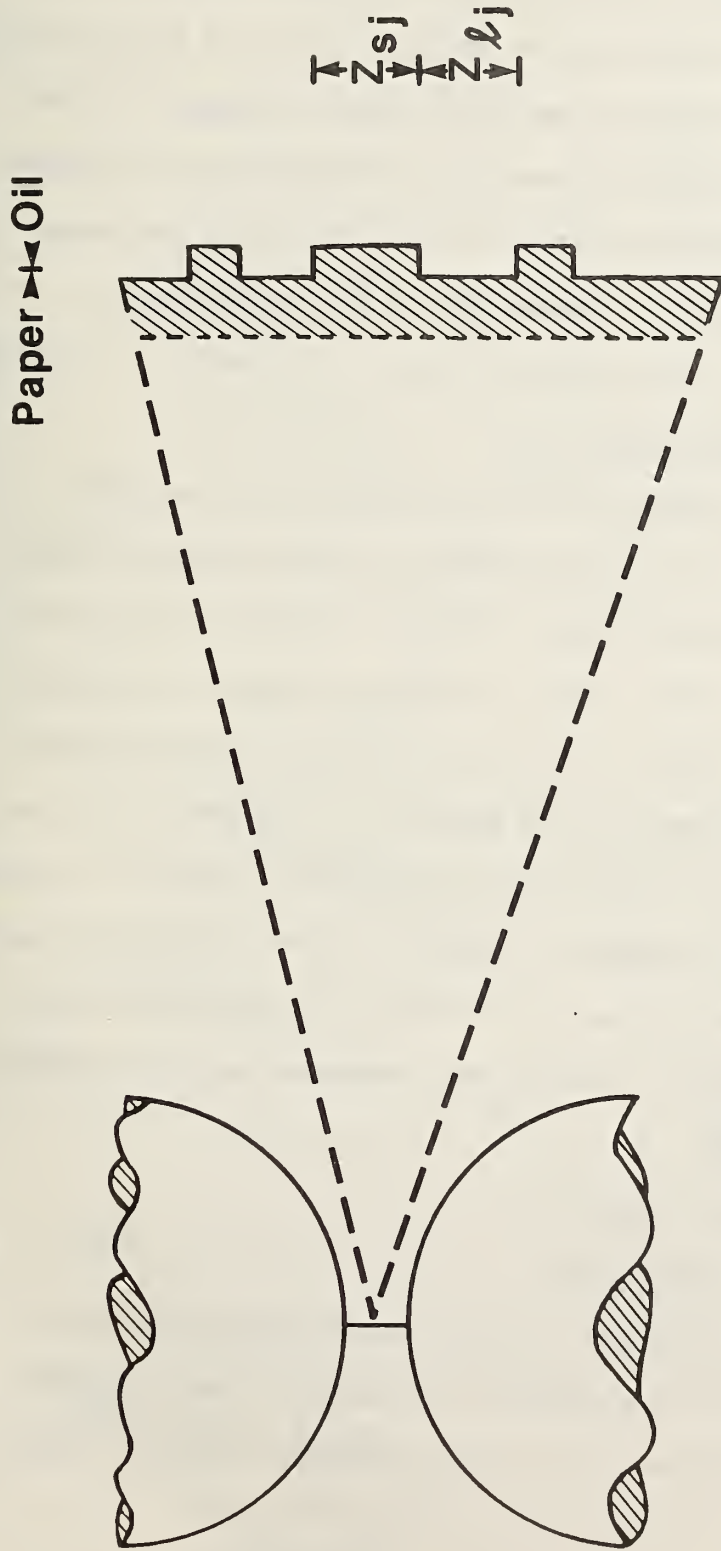
Figure 13. Idealized model of an oil-paper interface.

The fluid flow pattern was recorded using conventional flow visualization techniques. These measurements suggested that the fluid cavitation may contribute to a reduction of the breakdown in the vicinity of the interface.

The investigations summarized above indicate that, although insight has been gained, a comprehensive, coherent model of interfacial phenomena has yet to emerge. This report describes a consistent set of measurements which demonstrate the strengths and weaknesses of the present models. In addition, the significance of selected additional measurements is discussed.

4.2.3. Experimental Conditions

The electrode-interface geometries under consideration are shown in Fig. 14. The transformer oil used was commercial grade and was filtered to remove particles greater than 20 μm. The paper, typical of that used in transformers, was 0.062 mm thick. Care was taken to remove as much water as possible from the paper prior to its use in the tests. The paper was clamped by the split electrodes and held parallel to the field. The four electrodes were designed to be identical in all respects except, of course, for their differing radii of curvature. The four radii of curvature were chosen to be 1.6 mm, 3.2 mm, 6.4 mm, and 12.7 mm. The entire electrode structure is 25.4 mm in diameter. Tests were performed using both impulse and 60-Hz voltage waveforms.

4.2.4. Experimental Results

4.2.4.1. Introduction

Results are reported using all of the electrode geometries shown in Fig. 14. Most of the work concentrated on the two electrode structures having the larger radii of curvature, because they were the most technically significant.
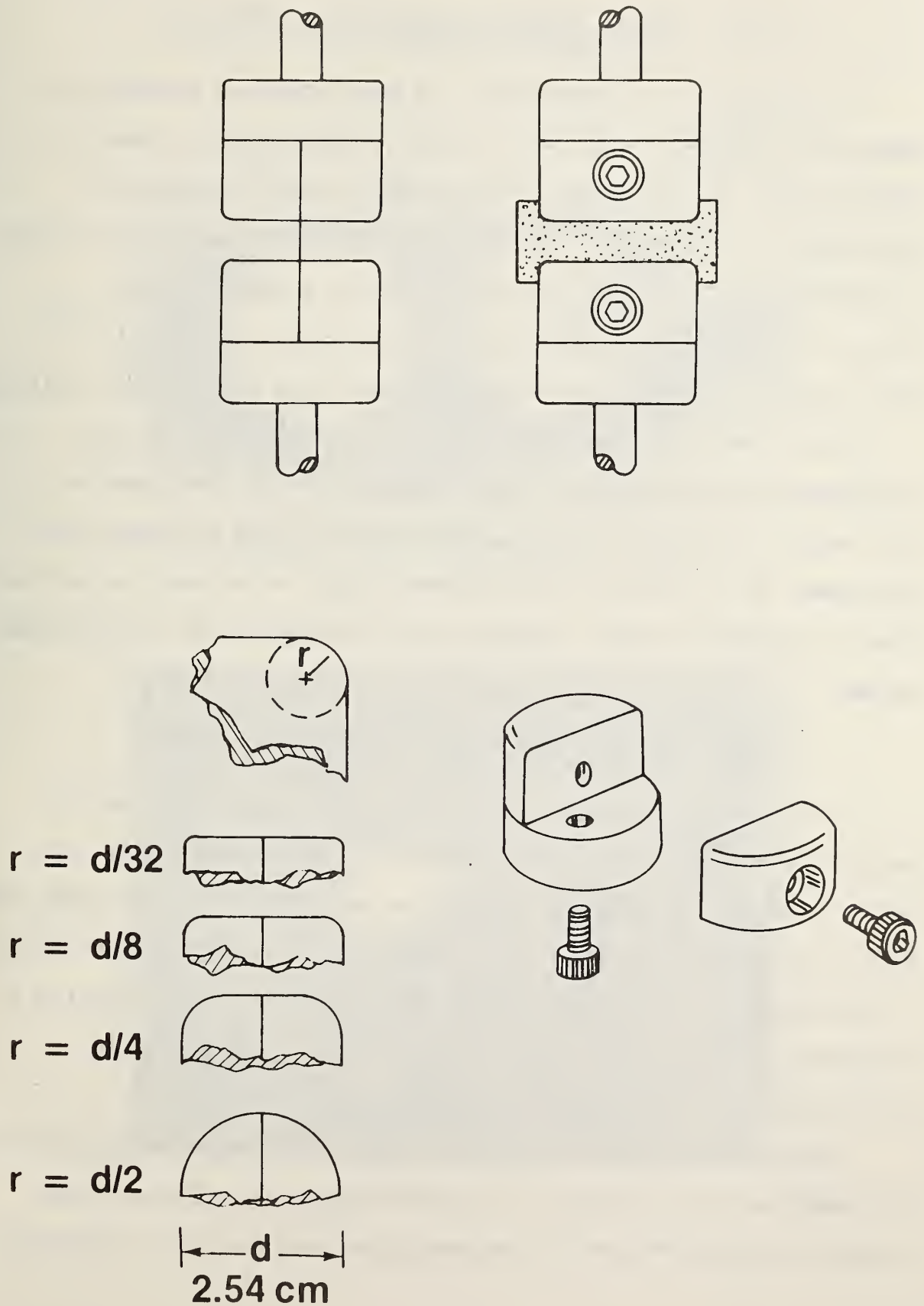
Figure 14. Electrode structure used to support paper. In the lower left
is shown, in approximate scale, the four electrodes used.

4.2.4.2. Results Using Electrodes Having a Radius of Curvature of 1.6 mm

A preliminary set of measurements was made without an interface, to characterize the behavior of the oil alone. A least-squares linear fit indicated that, on the average, the breakdown strength increased by approximately 0.4% per shot. For twenty breakdowns the mean field strength at breakdown was 310 kV. This result repeated in a number of data runs and is qualitatively consistent with previously published data.[8] This increase in breakdown strength is presumably due to electrode conditioning.

Results both with, and without, an interface indicated that the breakdown occurred preferentially near the edges of the electrodes for this radius of curvature. It was assumed that there was sufficient field enhancement in the vicinity of the electrode edges to dominate any interfacial effect. No further studies, therefore, were performed using this electrode system.

4.2.4.3. Results Using Electrodes Having a Radius of Curvature of 3.2 mm

In contrast to the data taken with the electrodes having a smaller radius of curvature, there was no tendency for the breakdown sites to be concentrated near the electrode edges. The photograph of the electrode surface after a series of breakdowns in shown in Fig. 15a. This photograph shows the relatively uniform distribution of discharge sites. A typical record of a breakdown location is shown in Fig. 15b. The paper sample joins the electrodes.

From these photographs it can be seen that there is no dominant preference for breakdown at the interface. To isolate interfacial effects, it was judged to be most efficient to concentrate the investigation on electrodes
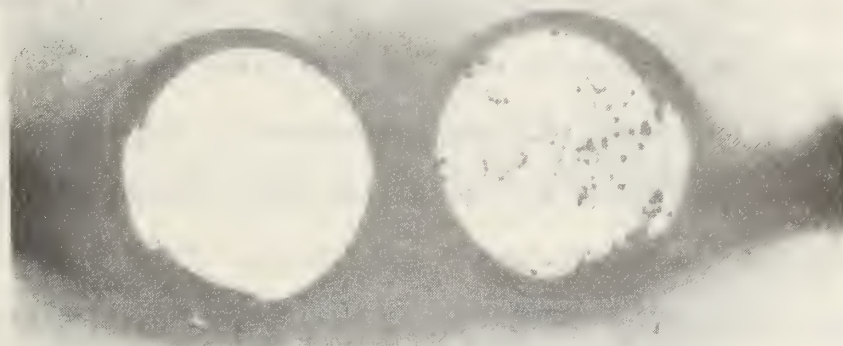
Figure 15. Upper photo shows the electrode surface after a number of
            breakdowns while the lower one shows a typical breakdown occurring
            away from the interface.

with even larger radii of curvature -- electrode systems in which the highest field strength is in the vicinity of the interface.

Two additional observations were made using the 3.2 mm electrodes. First the average breakdown field strength increased by about 20% as the radius of curvature was increased from 1.6 to 3.2 mm. This observation is consistent with the assumption that the data taken using the 1.6 mm electrodes were influenced by field enhancement at the electrode edges. Second, even though the oil was circulated and filtered, the test geometry resulted in hydrodynamically "dead" spots in the vicinity of the interface. After repeated breakdowns using the same interface, particulate contamination accumulated in the interfacial region.

4.2.4.4. Results Using Electrodes Having a Radius of Curvature of 6.4 mm

A summary of the data taken under impulse conditions is shown in Table 1. It should be emphasized that in this work, the differences among the average values is of the same order as the spread in readings under any one condition. It is difficult, therefore, to use these data to support the hypothesis that there is a significant difference between the breakdown strengths with and without an interface. This is particularly true if the data obtained using contaminated paper samples are eliminated. Although these data apparently contradict those presented by Wechsler and Riccitiello[2] they are consistent with the more recent experimental work by Taylor.[9] Taylor's data are summarized in Table 2. In an attempt to summarize the influence of the interface, Taylor calculated the "spacer efficiency" which was defined as the ratio of the breakdown strength of the solid-liquid combination to the breakdown strength of the liquid alone. Equation 42, which is based on the model of Wechsler and Riccitiello, relates the efficiency to the properties

Table 1:   Summary of Data for Uniform Field Breakdown

Experimental Conditions	Breakdown Field (kV/cm)	Breakdown Voltage (kV)	Efficiency
No interface, oil alone	529 ± 47	168 ± 15	--
Interface in place but breakdown not at interface	554 ± 50	176 ± 16	--
Breakdown at interface (all data)	482 ± 63	152 ± 20	0.91 ± 0.16
Breakdown at interface (exclude repeat breakdowns at same location)	494 ± 54	157 ± 17	0.93 ± 0.14
Breakdown at interface (exclude both repeated breakdowns and possible contaminated samples)	526 ± 38	167 ± 12	0.99 ± 0.11

Notes: 1. Uncertainties listed are one standard deviation.
2. The efficiency is the ratio of the breakdown voltage at the interface to the breakdown voltage with no interface in the system.

Table 2:   Summary of Interfacial Breakdown Results Reported by Taylor

Experimental Conditions	Field Strength (kV/cm)	Efficiency
No interface, oil alone	480 ± 39	--
Oil-polycarbonate interface	454 ± 44	0.95 ± 0.13
Oil-pressboard interface	401 ± 57	0.84 ± 0.16
Oil-polyphenylene oxide interface	463 ± 33	0.96 ± 0.11

Notes: 1. The uncertainties listed are one standard deviation.

2. The efficiency is the ratio of breakdown field strength at the interface to the breakdown field strength with no interface in the system.

of the liquid and the solid. In Tables 1 and 2, the efficiencies are calculated along with their uncertainties. The uncertainty is taken as the square root of the sum of the squares of the uncertainties in the two quantities which are divided to calculate the efficiency.

Using the same electrode system, data were also taken using 60-Hz voltage waveforms. As was the case with impulse voltages, however, the data indicate no obvious enhancement of the breakdown probability in the vicinity of the interface.

4.2.4.5. Results Using Electrodes Having a Radius of Curvature of 12.7 mm

In an attempt to drive the breakdown to the interface, a split sphere-sphere electrode geometry was employed. In such a system the maximum field strength occurs at the interface. Because of practical difficulties in assembling the electrode structure with the paper sample in place, a misalignment of the electrode halves was frequently observed. This misalignment was generally less than 2% of the gap spacing. It was assumed that this misalignment would increase the probability of breakdown at the interface because of field enhancement. The data, however, indicate the results were largely insensitive to this parameter. The data are summarized in Table 3.

There is also selective data analysis in Table 3. Those values for breakdown at the interface in which the breakdown occurred the first time that voltage was applied were averaged separately. The motivation for this was concern that breakdowns away from the interface would deposit particulate debris on or near the interface. As can be seen in Table 3, the breakdown voltage was slightly higher for interfacial breakdowns on virgin systems than for non-virgin systems. The difference, however, was too small to be considered significant with the limited amount of data that were taken. The 60-Hz breakdown data are summarized in Table 4.

Table 3:   Summary of Impulse Breakdown Data for Sphere-Sphere Electrodes

Experimental Conditions	Breakdown Voltage kV	Efficiency
No interface, oil alone	173 ± 19	--
Interface in place but breakdown not at interface	172 ± 20	--
Breakdown at interface (all data)	170 ± 26	0.98 ± 0.19
Breakdown at interface (virgin system)	173 ± 27	1.00 ± 0.19

Notes: 1. Uncertainties listed are one standard deviation.
2. The efficiency is the ratio of the breakdown voltage at the interface to the breakdown voltage with no interface in the system.

Table 4:   Summary of 60-Hz Breakdown Data for Sphere-Sphere Electrodes

Experimental Conditions	Breakdown Voltage kV	Efficiency
Interface in place but breakdown not at interface	108 ± 11	--
Breakdown at interface	111 ± 6	1.03 ± 0.12

Notes: 1. Uncertainties listed are one standard deviation.
2. Efficiency is the ratio of the voltage for breakdown at the interface to the voltage for breakdown not at the interface.

4.2.4.6. Conclusions

It is widely assumed that in many situations the interface between the solid and the liquid insulation is the point in a complex system at which breakdown would occur. The data reported here do not support that conventional wisdom. From these data, which were taken using a carefully prepared, paper-oil interface structure, it was concluded that the breakdown will not necessarily occur at the interface. Similarly, the breakdown voltage for breakdown at the interface is not necessarily lower than the voltage at which breakdowns occur away from the interface.

The work indicated, however, that it seemed a relatively simple matter to force the breakdown to the interface and at the same time reduce the breakdown voltage. It is likely that interfacial breakdown will occur if the paper is not carefully dried or if many gaseous voids are left in or on the paper. The influence of moisture and the influence of gaseous voids are recognized in the process of manufacture of high voltage apparatus. Procedures have been developed, and are being followed, to minimize the impact of these factors on the finished piece of apparatus. If moisture and air are the dominant restrictions to the increase of the breakdown strength of practical apparatus, then future research and development is needed in this area. The detection of the air and water content of the materials in the devices must be improved and materials must be developed with lower sensitivity to the deleterious effects of these quantities.

It is likely that additional factors must be considered. Experience has demonstrated that breakdown voltages are distributed statistically. It is, therefore, reasonable to assume that the breakdown voltage at the interface and the breakdown voltage in the fluid are each statistically

distributed. In fact, Taylor's[9] data support the hypothesis that these two
voltages are described by different distributions. If that is true, a critical
parameter is the normalization of the distributions of the breakdown probabilities
in the two cases. Although such a scaling parameter has also been suggested
by the data of Nelson, et al.,[10] it must be emphasized that the existence of
such a parameter has not been verified experimentally. Carefully controlled
experiments are required to determine both the breakdown voltage and breakdown
location as the ratio of the interfacial surface area (or volume) to the
stressed oil volume is systematically varied. These tests will provide
information required to design model tests which simulate the behavior of
practical apparatus.

4.3. Prebreakdown Phenomena in Transformer Oil

4.3.1. Introduction

Both cathode and anode streamers have been observed in transformer
oil under divergent field conditions and under uniform field conditions.
The temporal evolution of these processes has, however, not been studied
using uniform applied fields. Measurements were, therefore, performed on
the temporal behavior of both cathode and anode processes. Under the
conditions of these experiments, the cathode streamer development was a
three-step process while the anode streamer was a two-step process. Two-step
cathode processes have been previously reported for divergent and for
uniform fields.[11]

4.3.2. Experimental Conditions

For these measurements, a commercial grade of transformer oil was used
with a sphere-sphere electrode geometry. The spheres had a diameter of 2.5 cm
and were spaced so that the gap between them measured 0.32 cm. The streamer
propagation was recorded using an image converter camera having an exposure
time of 10 ns and a time of 50 ns between consecutive photographs. A

pulsed (pulse duration is approximately 6 µs) argon-ion laser was used for illumination. In this discussion, events are classified as subsonic (or supersonic) if their propagation velocity is less than (or greater than) the speed of sound in the fluid. The speed of sound is assumed to be the propagation velocity of the shock wave which emanates from the breakdown event.

4.3.3. Experimental Results

Figure 16 shows two cathode phenomena in the first four frames. The small "bushy" streamer coming from the surface of the cathode is a subsonic event. Other photographs show that this type of event has an average velocity of $(2.4 \pm 0.4) \times 10^4$ cm/s.[1] (The velocities listed are assumed to be accurate to ±20%.) In the same frames an event with a higher velocity is also shown. This streamer has an average velocity of 1.5×10^5 cm/s which is at or slightly greater than sonic speed. Some acceleration of this streamer may be occurring. In the fifth frame a supersonic event initiates and has bridged the gap by the seventh frame. This supersonic streamer has an average velocity of 4×10^6 cm/s which is about 25 times the sonic speed.

Figure 17 shows the analogous development of an anode streamer. A supersonic, bush-like structure initiates at the anode (frame 5) and grows at a rate of 4×10^5 cm/s which is about 2.5 times the sonic speed. As the streamer propagates it shifts to a faster propagation mode and bridges the gap in about 50 ns. This second anode event has a velocity of 4.5×10^6 cm/s -- 30 times sonic speed.

These preliminary data demonstrate a number of significant features. For example, these data suggest that, as is the case with divergent-field electrode systems, only the cathode streamer has a subsonic propagation mode.
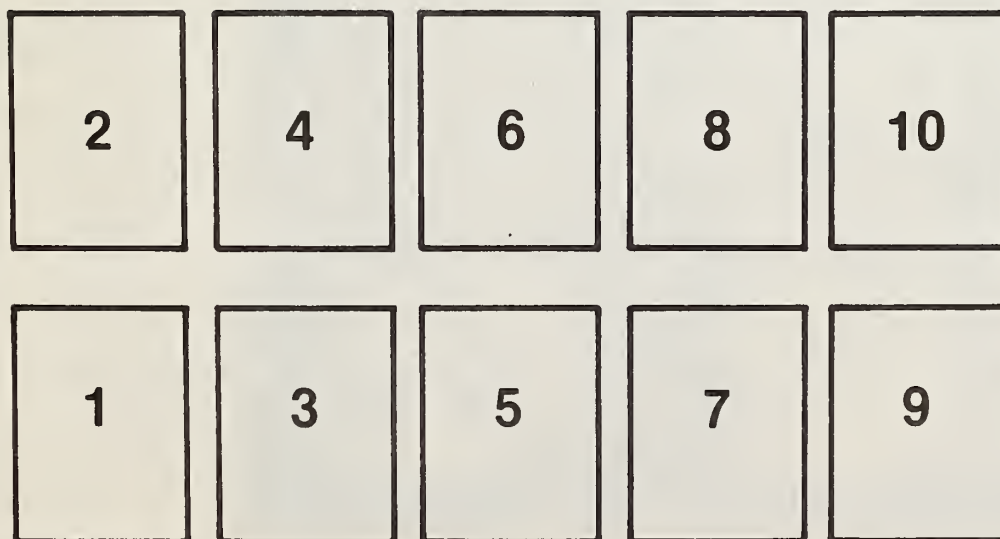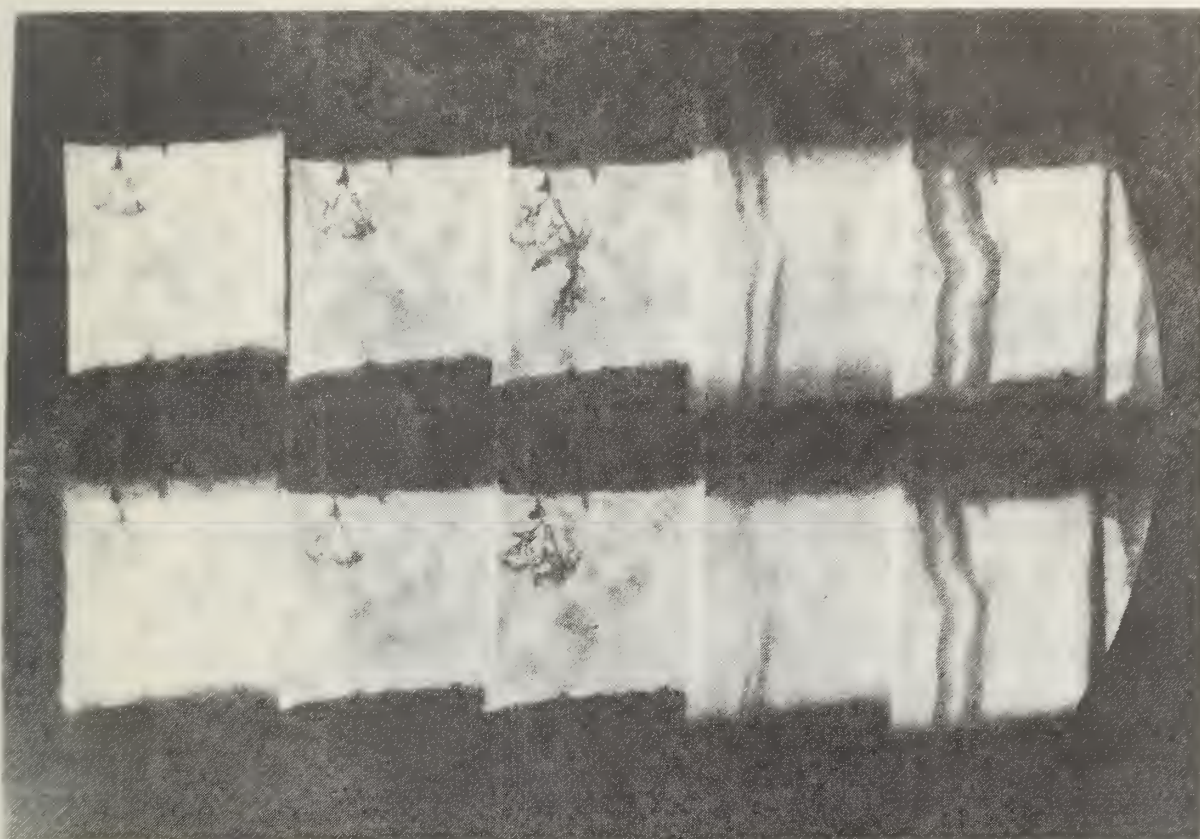
IMAGE—CONVERTER CAMERA
FRAMING SEQUENCE

Figure 16.   Cathode streamers are shown in the upper photo while the lower drawing is the framing sequence.   Each frame is a 10 ns exposure with 50 ns between frames.

Figure 17. Typical streamer initiating from the anode.

It is also clear that both anode and cathode processes can independently be responsible for breakdown in uniform electric fields. Figure 18 shows simultaneous development of both anode and cathode streamers, with the anode streamer responsible for breakdown. Another interesting feature of this photograph is the cylindrical shockwave emanating from the "frozen" cathode streamer. From these data, it is inferred that the streamer propagated much faster than sonic speed until it was stopped when an anode streamer bridged the gap, thus reducing the potential difference between the electrodes. Figure 19 shows the unusual situation in which the anode and cathode streamers caused breakdown by meeting in the midgap region.

4.4. Dielectrophoretic Phenomena

4.4.1. Introduction

Basic research, intended to support the study of liquid-solid interfaces, was performed in the area of dielectric constant measurement using dielectrophoretic (DEP) levitation. The DEP technique offers the potential advantage that it can be used to measure directly the dielectric constant of the small particles which commonly occur in practical apparatus. The investigation was to refine the analysis of the sensitivity of the technique for dielectric constant determinations, to determine effects attributable to particle size and shape, to develop apparatus to measure the dielectric constant and to perform the measurements.

With this approach, all measurements are made relative to a standard liquid with a well-known dielectric constant. The cell is calibrated by levitating a small gas bubble in the standard liquid at a fixed position. Throughout this section (Section 4.4) the subscript "C" is used to indicate parameters associated with the calibration fluid, process or measurement. The dielectric constant of spherical particles is determined by levitating them in the standard liquid. Similarly, the dielectric constant of a liquid
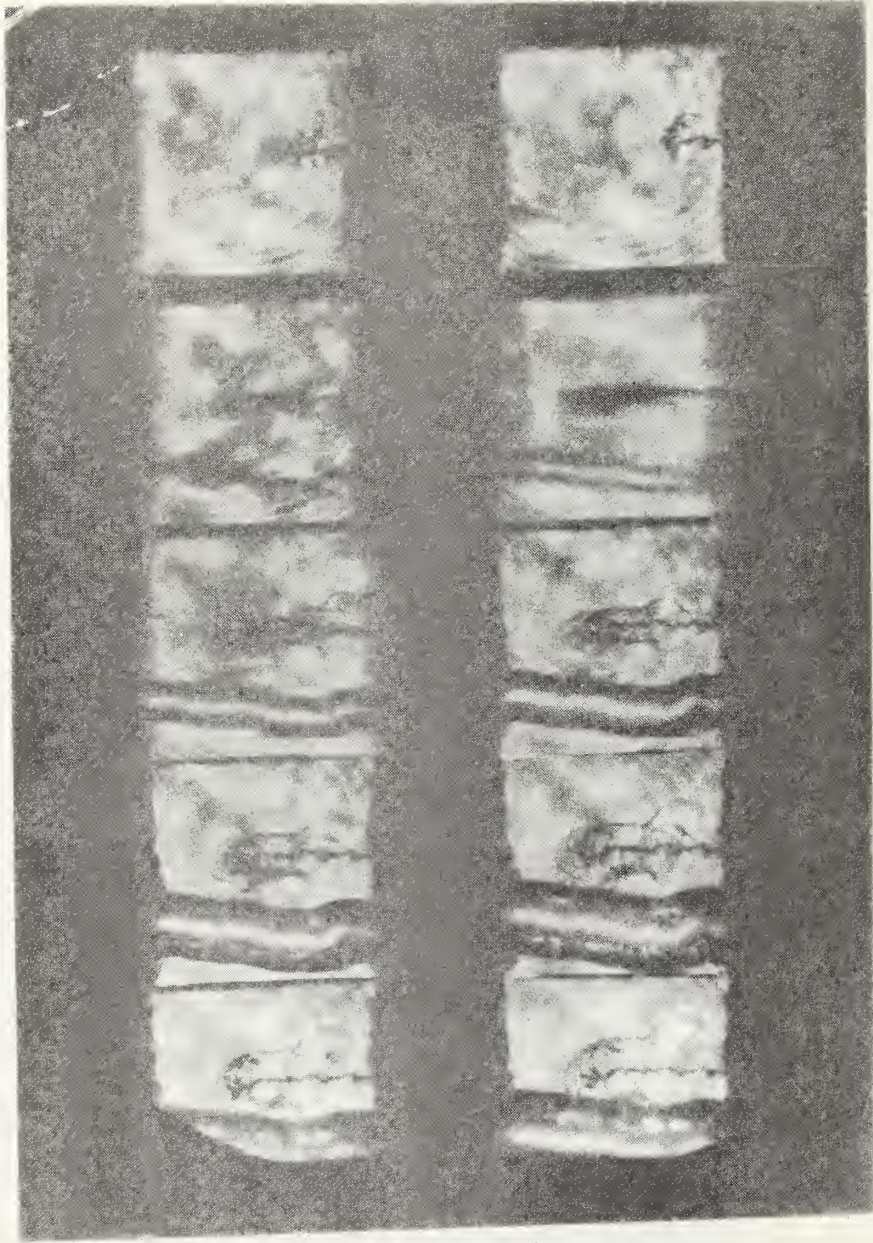
Figure 18. Streamers initiating from both anode and cathode with breakdown caused by anode streamer.
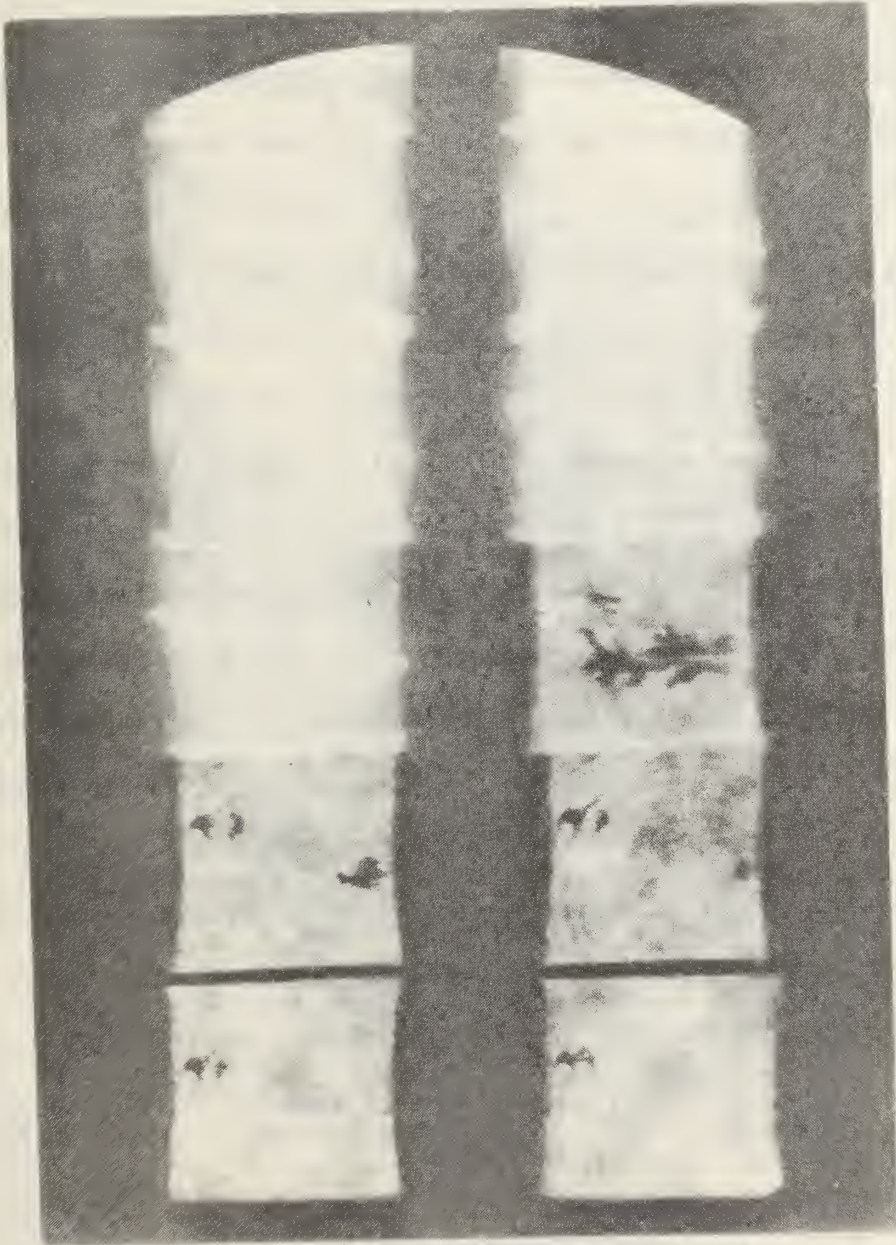
Figure 19. Example of breakdown being caused by a streamer from the anode and one from the cathode meeting in the mid-gap region.

can be determined by levitating a bubble at the same position using the calibration liquid and the unknown fluid alternately in the same test cell.

4.4.2. Sensitivity

The sensitivity analysis is essentially complete; the important contributions to measurement uncertainty have been identified and sensitivity functions have been obtained. The effect of positioning errors on the measurement has also been investigated. Some knowledge of the spatial dependence of the electric field is required to estimate the required sensitivity functions. For analysis purposes, the analytical solution for a charged ring mounted with its axis normal to a conducting ground plane (Fig. 20) has been used as a model of the electric field distribution. The solution provides the field intensity and various derivatives needed to estimate the effects of positioning errors and the deviations from sphericality for either a bubble or a particle. The validity of the charged ring/ground plane model for the cusped electric field has been tested experimentally. One important conclusion drawn from the analysis is that the uncertainty in the dielectric constant measurement is a function of the position at which the bubble or particle is levitated. For most typical situations, it is best to levitate the bubble or particle near the release point -- the release point separates the region along the symmetry axis in which levitation is possible from that in which it is not.

A summary of the error analysis is found in Table 5. These expressions relate the uncertainty $|\frac{\delta \kappa}{\kappa}|$ in the measured dielectric constants for liquids and solids to the uncertainties in the important fluid parameters and physical measurements. Because the dielectrophoretic levitation scheme is a relative measurement (relative to a standard), the
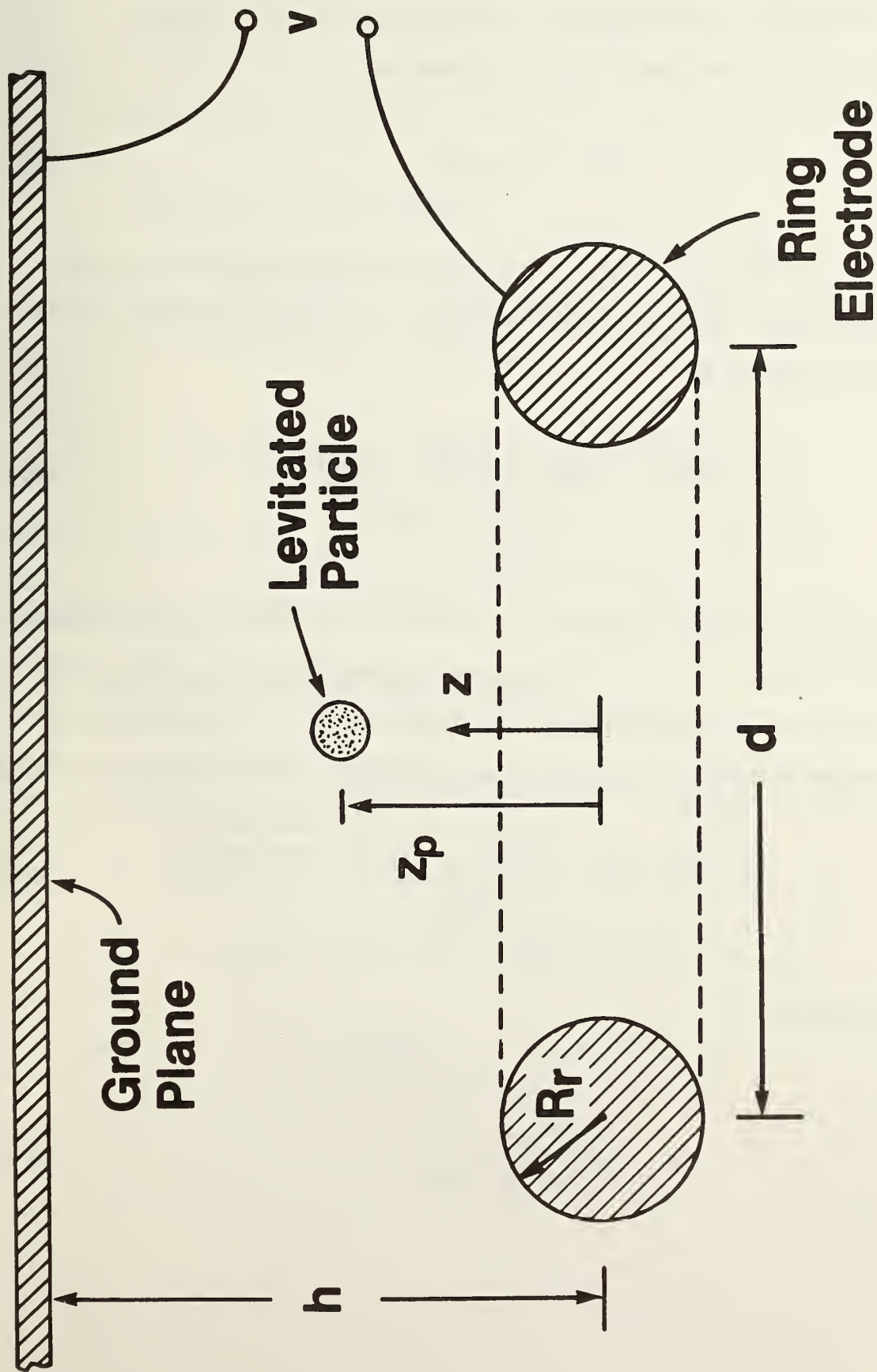
Figure 20. Ring-plane geometry used to provide an approximate analytical model for the cusped electric field.

uncertainties in the cell calibration exercise must be considered. This cell calibration is quantified by a geometric term $K(z)$, which is defined by Kallio and Jones[12] with the equation,

$$\nabla E^2 = \frac{2}{3} g K(z) V^2 \hat{z} \tag{43}$$

where E is the electric field, g is the gravitational acceleration, and V is the voltage. In the calibration exercise, $K(z)$ is determined at the levitation point z_p by

$$K(z_p) = \frac{|\rho_{2c} - \rho_{1c}|(\kappa_{2c} - 2\kappa_{1c})}{\varepsilon_0 \kappa_{1c}|\kappa_{1c} - \kappa_{2c}|V_c^2} \tag{44}$$

where V_c is the voltage required to levitate an air bubble in the standard dielectric liquid at $z=z_p$, ρ_1 and ρ_2 are the densities and κ_1 and κ_2 the respective dielectric constants of the liquid and air. The unknowns are expressed as functions of K plus other parameters. Specifically, for liquids,

$$\kappa_1 = \frac{KV^2\varepsilon_0\kappa_2 + 2\Delta\rho + \sqrt{(KV^2\varepsilon_0\kappa_2 + 2\Delta\rho)^2 + 4KV^2\Delta\rho\varepsilon_0\kappa_2}}{2KV^2\varepsilon_0} \tag{45}$$

and for solids

$$\kappa_2 = \frac{\kappa_1(KV^2\varepsilon_0\kappa_1 - 2\Delta\rho)}{KV^2\varepsilon_0\kappa_1 + \Delta\rho} \quad . \tag{46}$$

Table 5: Summary of sensitivity analysis

CALIBRATION

$$\left|\frac{\delta K}{K}\right| = \left|\frac{\delta\Delta\rho_c}{\Delta\rho_c}\right| + 2\left|\frac{\delta V_c}{V_c}\right| + \left\{\frac{\kappa_{2c}}{2\kappa_{1c}+\kappa_{2c}} + \frac{\kappa_{2c}}{\kappa_{1c}-\kappa_{2c}}\right\}\left|\frac{\delta\kappa_{2c}}{\kappa_{2c}}\right| + \left\{\frac{2\kappa_{1c}}{2\kappa_{1c}+\kappa_{2c}} - \frac{\kappa_{1c}}{\kappa_{1c}-\kappa_{2c}} - 1\right\}\left|\frac{\delta\kappa_{1c}}{\kappa_{1c}}\right|$$

LIQUID DIELECTRIC CONSTANT MEASUREMENT

$$\left|\frac{\delta\kappa_1}{\kappa_1}\right| = 2S_\kappa^{\kappa_1}\left[\frac{\dfrac{h^4}{V^2}\dfrac{d^2E_o^2}{dz^2}}{\dfrac{h^3}{V^2}\dfrac{dE_o^2}{dz}}\right]\left|\frac{\delta z_o}{h}\right| + S_\kappa^{\kappa_1}\left[\frac{\dfrac{h^2}{V^2}E_o^2}{\dfrac{h^3}{V^2}\dfrac{dE_o^2}{dz}}\right]\left|\frac{.6(\kappa_{1c}-\kappa_{2c})^2 ghR_{oc}\Delta\rho_c}{(2\kappa_{1c}+\kappa_{2c})^2\sigma_c} - \frac{.6(\kappa_1-\kappa_2)^2 ghR_o\Delta\rho}{(2\kappa_1+\kappa_2)^2\sigma}\right|$$

$$+ S_\kappa^{\kappa_1}\left|\frac{\delta K}{K}\right| + (S_\kappa^{\kappa_1}+1)\left|\frac{\delta\kappa_2}{\kappa_2}\right| + S_\kappa^{\kappa_1}\left|\frac{\delta\Delta\rho}{\Delta\rho}\right| + 2S_\kappa^{\kappa_1}\left|\frac{\delta V}{V}\right|$$

$$S_\kappa^{\kappa_1} = a\left[\frac{1+(a+4)(a^2+8a+2)^{-\frac{1}{2}}}{(a+2)+(a^2+8a+2)^{\frac{1}{2}}}\right], \quad a = \frac{\kappa_2(2\kappa_1+\kappa_2)}{\kappa_1(\kappa_1-\kappa_2)}$$

SOLID SPHERICAL DIELECTRIC PARTICLE MEASUREMENT

$$\left|\frac{\delta\kappa_2}{\kappa_2}\right| = 2S_\kappa^{\kappa_2}\left[\frac{\dfrac{h^4}{V^2}\dfrac{d^2E_o^2}{dz^2}}{\dfrac{h^3}{V^2}\dfrac{dE_o^2}{dz}}\right]\left|\frac{\delta z_o}{h}\right| + S_\kappa^{\kappa_2}\left|\frac{.6(\kappa_{1c}-\kappa_{2c})^2 ghR_{oc}\Delta\rho_c}{(2\kappa_{1c}+\kappa_{2c})^2\sigma_c}\left(\frac{\dfrac{h^2}{V^2}E_o^2}{\dfrac{h^3}{V^2}\dfrac{dE_o^2}{dz}}\right) - \frac{4(\kappa_1-\kappa_2)\alpha}{5(2\kappa_1+\kappa_2)}\right|$$

$$+ S_\kappa^{\kappa_2}\left|\frac{\delta K}{K}\right| + (S_K^{\kappa_2}+1)\left|\frac{\delta\kappa_1}{\kappa_1}\right| + S_K^{\kappa_2}\left|\frac{\delta\Delta\rho}{\Delta\rho}\right| + 2S_K^{\kappa_2}\left|\frac{\delta V}{V}\right|$$

$$S_K^{\kappa_2} = \frac{3a(\kappa_1/\kappa_2)}{\left(a\dfrac{\kappa_1}{\kappa_2}-2\right)\left(a\dfrac{\kappa_1}{\kappa_2}+1\right)}, \quad \alpha = \gamma - 1$$

Accurate determination of K is, therefore, crucial to overall measurement accuracy, and so Table 5 contains an expression for $|\frac{\delta K}{K}|$.

The various implications of the results in Table 5 are best illustrated by an example. Below are listed the principal assumptions and results of calculating the various sensitivity functions for (i) the calibration exercise, i.e., experimental determination of K, (ii) measurement of a typical liquid dielectric constant κ_1, and (iii) measurement of a typical solid dielectric constant κ_2.

(i) Cell calibration (determination of K)

. test cell dimensions, h=1 cm (c.f. Fig. 20)

. spatial resolution, ± 8 μm

. calibration system: 100 μm air bubble in carbon tetrachloride

liquid medium (CCl_4): κ_{1c} = 2.228 ± 0.0005

@ 25 °C ρ_{1c} = 1594.0 ± 0.05 kg/m^3

σ = 0.02695 N/m

air bubble : κ_{2c} = 1.000590 ± 5 · 10^{-7}

@ 25 °C,
1 x 10^5 Pa ρ_{2c} = 1.185 ± 0.0005 kg/m^3 ;

where σ is the surface tension.

For the conditions summarized above, the uncertainty in K is

$$|\frac{\delta K}{K}| = 0.05\% + 2\ |\frac{\delta V_c}{V_c}|$$ (47)

where $|\frac{\delta V_c}{V_c}|$ is the uncertainty in the calibration voltage measurement.

(ii) Unknown Liquid Measurement

Here, an estimate of the uncertainty involved in measurement

of the dielectric constant of a common liquid dielectric is made.
In this example, a silicone oil is chosen which has a
published value of κ_1 = 2.75.

. same test cell

. spatial resolution (± 8 μm)

. measurement system: 100 μm air bubble in silicone oil

    liquid medium (unknown): κ_1 ~ 2.75

        @ 25 °C ρ_1 = 972 ± 0.5 kg/m^3

                                  σ = 0.0212 N/m

    air bubble :   same as calibration .

For the above assumed parameters and uncertainties, the uncertainty in
the unknown κ_1 is determined to be

$$|\frac{\delta\kappa_1}{\kappa_1}| = 0.32\% + 0.58 \ |\frac{\delta K}{K}| + 1.16 \ |\frac{\delta V}{V}| \quad . \tag{48}$$

Using Eq. 47,

$$|\frac{\delta\kappa_1}{\kappa_1}| = 0.35\% + 1.16 \ [|\frac{\delta V_c}{V_c}| + |\frac{\delta V}{V}|] \tag{49}$$

where $|\frac{\delta V}{V}|$ is the uncertainty in the voltage measurement on the unknown. The 0.35% error in Eq. 49 encompasses all uncertainties (bubble elongation, spatial resolution, etc.), except for those associated with the voltage measurements. Equation 49 can be used to examine the effect of voltage precision on the overall uncertainty of κ_1. Table 6 contains some of these results.

Table 6. Effect of Voltage Precision on $|\frac{\delta \kappa_1}{\kappa_1}|$

$|\frac{\delta V}{V}|$, $|\frac{\delta V_c}{V_c}|$	$|\frac{\delta \kappa_1}{\kappa_1}|$
1%	2.7%
0.5%	1.5%
0.1%	0.6%
0.01%*	0.37%

*lower limit on rms voltage measurement precision

Obviously, very little benefit is gained in reducing the voltage error from 0.1% to 0.01%; however, the lower limit of 0.01% for rms voltage measurement may be achieved without too much expense. Thus, for liquid measurement, overall accuracy is limited to about 0.4%. It may be shown that the chief contribution to this value (0.4%) is spatial resolution. Smaller bubbles ($\sim$ 50 μm) might permit an additional reduction to $|\frac{\delta\kappa_1}{\kappa_1}| \sim 0.2\%$, but it is difficult to imagine further improvements.

(iii) Unknown Solid Measurement

In this example, solid polystyrene spheres (100 μm) are chosen as the unknown particles. It is assumed that they are to be levitated in capacitor-grade castor oil. The nominal dielectric constant for polystyrene is κ_2 = 2.3. The various assumptions, etc., are summarized below.

. same test cell

. spatial resolution: $\pm$8 μm

. measurement system: 100 μm polystyrene particles in caster oil

   liquid medium (caster oil): κ_1 = 4.74

   @ 25 °C ρ_1 = 958. $\pm$ 0.5 kg/m^3

   solid particle (unknown): κ_2 $\simeq$ 2.38

   ρ_2 = 1055. $\pm$ 0.5 kg/m^3 .

The solid particles are assumed to exhibit prolate spheroidal deviations from ideal sphericity. If γ is defined to be the ratio of the semi-major axis to the semi-minor axis, the uncertainty of κ_2 becomes

$$\left|\frac{\delta\kappa_2}{\kappa_2}\right| = 0.37\% + 0.132(\gamma-1)\% + 0.827\left|\frac{\delta K}{K}\right|$$

$$+ 1.83\left|\frac{\delta\kappa_1}{\kappa_1}\right| + 0.83\left|\frac{\delta\Delta\rho}{\Delta\rho}\right| + 1.65\left|\frac{\delta V}{V}\right| \quad .$$

(50)

In those cases in which the densities ρ_1 and ρ_2 are quite close, in solid-liquid measurements for example, $\Delta\rho = |\rho_2 - \rho_1|$ is a significant parameter. Using Eq. 47, we obtain

$$\left|\frac{\delta\kappa_2}{\kappa_2}\right| = 0.41\% + 0.13|\gamma-1\%| + 1.83\left|\frac{\delta\kappa_1}{\kappa_1}\right| + 0.83\left|\frac{\delta\Delta\rho}{\Delta\rho}\right|$$

(51)

$$+ 1.65\left[\left|\frac{\delta V_c}{V_c}\right| + \frac{\delta V}{V}\right] \quad .$$

Several factors conspire to limit the precision of κ_2 measurement. Values for $\left|\frac{\delta\kappa_2}{\kappa_2}\right|$ obtained by using Eq. 51 are tabulated in Table 7, where it is assumed that $\left|\frac{\delta V_c}{V_c}\right| = \left|\frac{\delta V}{V}\right|$ and $\left|\frac{\delta\Delta\rho}{\Delta\rho}\right| = 1\%$.

Table 7. Effect of Parameters on $\left|\frac{\delta\kappa_2}{\kappa_2}\right|$

			$\left|\frac{\delta V}{V}\right|$		
			1%	0.1%	.01%*
$\left|\frac{\delta\kappa_1}{\kappa_1}\right|$	2%	$\gamma-1 = 10\%$	9.5%	6.4%	6.3%
		$\gamma-1 = 1\%$	8.3%	5.4%	5.1%
	1%	$\gamma-1 = 10\%$	7.7%	4.7%	4.4%
		$\gamma-1 = 1\%$	6.5%	3.5%	3.2%
	** 0.1%	$\gamma-1 = 10\%$	6.0%	3.1%	2.8%
		$\gamma-1 = 1\%$	4.9%	1.9%	1.6%

*lower limit on rms voltage measurement precision

**reasonable limit on liquid dielectric measurement precision using conventional capacitance cell methods.

The results of Table 7 are instructive because they provide guidance for the specification of the measurement precision required for solid dielectric particles. For example, it can be inferred that voltage precision greater than about 1.0% is unwarranted.

4.4.3. Dielectric Constant Measurements

A levitation cell was constructed and has been used to measure dielectric constant for some readily available dielectric liquids. The standard liquid has been chosen to be a silicone oil. The results are compared to measurements made with a standard capacitance cell. The results are tabulated below in Table 8. Data on liquid density are also provided, because they are needed in the equation used to compute the unknown dielectric constant.

Table 8.   Comparison of Measured Dielectric Constant Results
and Published Values

| Fluid | Dielectric constant values | | | Density | |
	Levitation cell result	Capacitance cell result	Published value	Measured result	Published value
DC-702 silicone oil	calibration	2.79	2.78	1.086	1.071
Castor oil (DI grade)	4.79 - 4.81	4.60	4.67	0.963	0.958
Corn oil	3.22	3.20	3.1	0.918	0.914
Transformer oil		2.25	2.23	0.887	0.893

These measurements of the dielectric constants of liquids demonstrate that the system operates as intended.

4.4.4. Circle Aperture Electrode Geometry

The experimental work has indicated that an electrode geometry is needed which is easy to fabricate in small sizes. The result of this quest has been the "circle aperture" arrangement shown in Fig. 21. The geometry consists of three parallel electrodes. One electrode, in the center features a circular hole of diameter d. This aperture forms the axisymmetric cusped electric field which permits levitation of particles or bubbles. The circular aperture levitator behaves in most respects like the ring-plane geometry. The locus of stable levitation equilibrium points exhibits a release point at the intense electric field end, above which no levitation is possible. Under certain conditions, the lower limit of the locus of equilibrium points is defined by a field null. However, under some conditions, the lower limit is discovered to be a point of marginal radial stability. As the voltage is increased a levitated particle moves toward this point and when the particle reaches the point, it becomes marginally stable to radial displacements. The result is that the particle slowly drifts off to the side and is lost.

The electric field for the circular aperture is approximated by the result used in electron optics theory[13]

$$E_z = \frac{E_2 + E_1}{2} + \frac{(E_2 - E_1)}{\pi} \left\{ \tan^{-1}\left(\underline{z}/\underline{a}\right) + \frac{\underline{z}/\underline{a}}{(\underline{z}/\underline{a})^2 + 1} \right\} \qquad (52)$$

where $\underline{z} = z/h$ and $\underline{a} = d/2h$ and h and d are defined in Fig. 22. E_1 and E_2 are the uniform electric fields for $z < 0$ and $z > 0$, respectively, far from the aperture.

Limited experimental measurements with the circular aperture geometry have been obtained for the case $E_1 = 0$. The results are shown in Fig. 22.
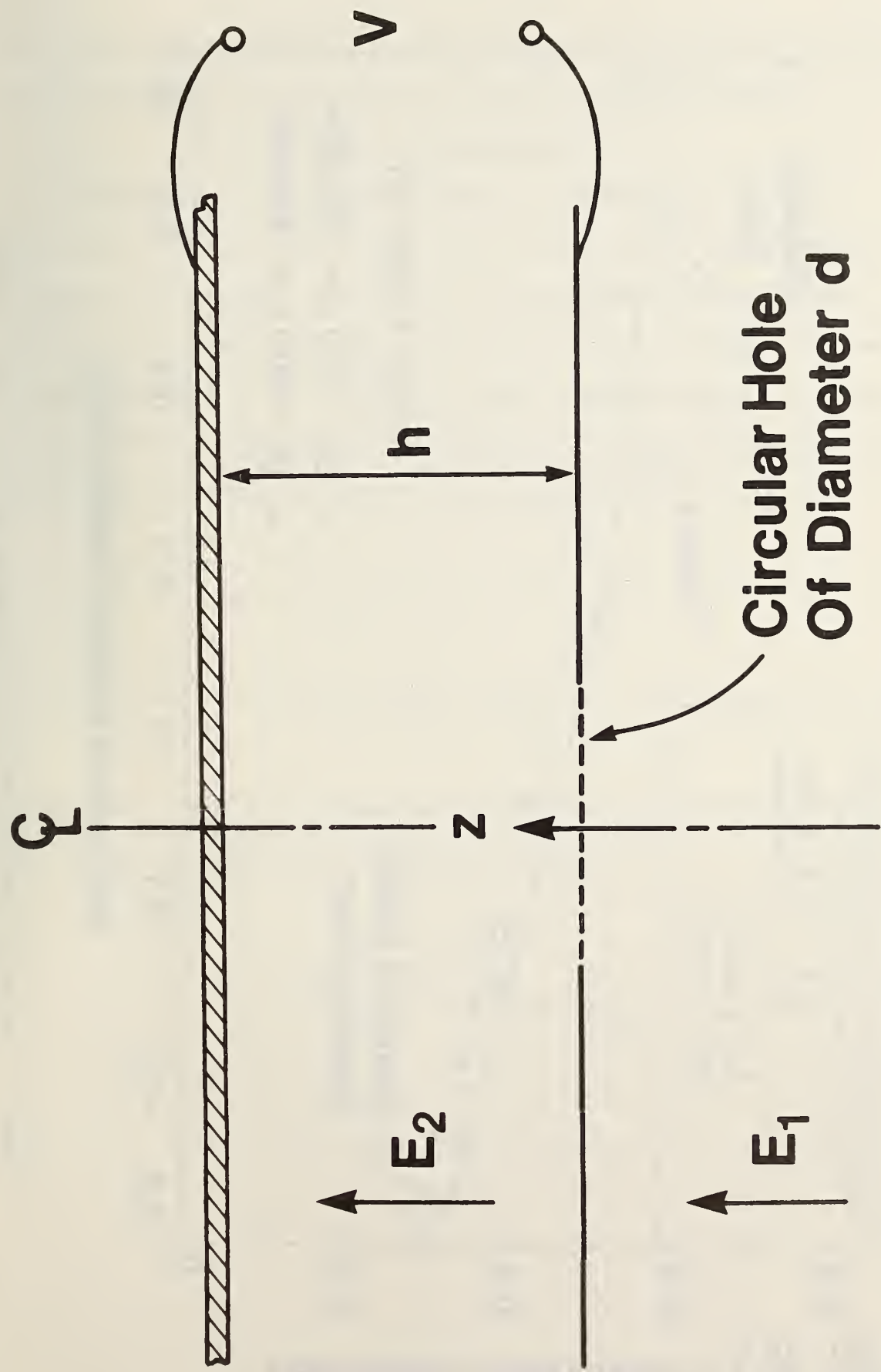
Figure 21. Axisymmetric circular aperture geometry. The grounded electrode needed to produce E_1 is not shown.
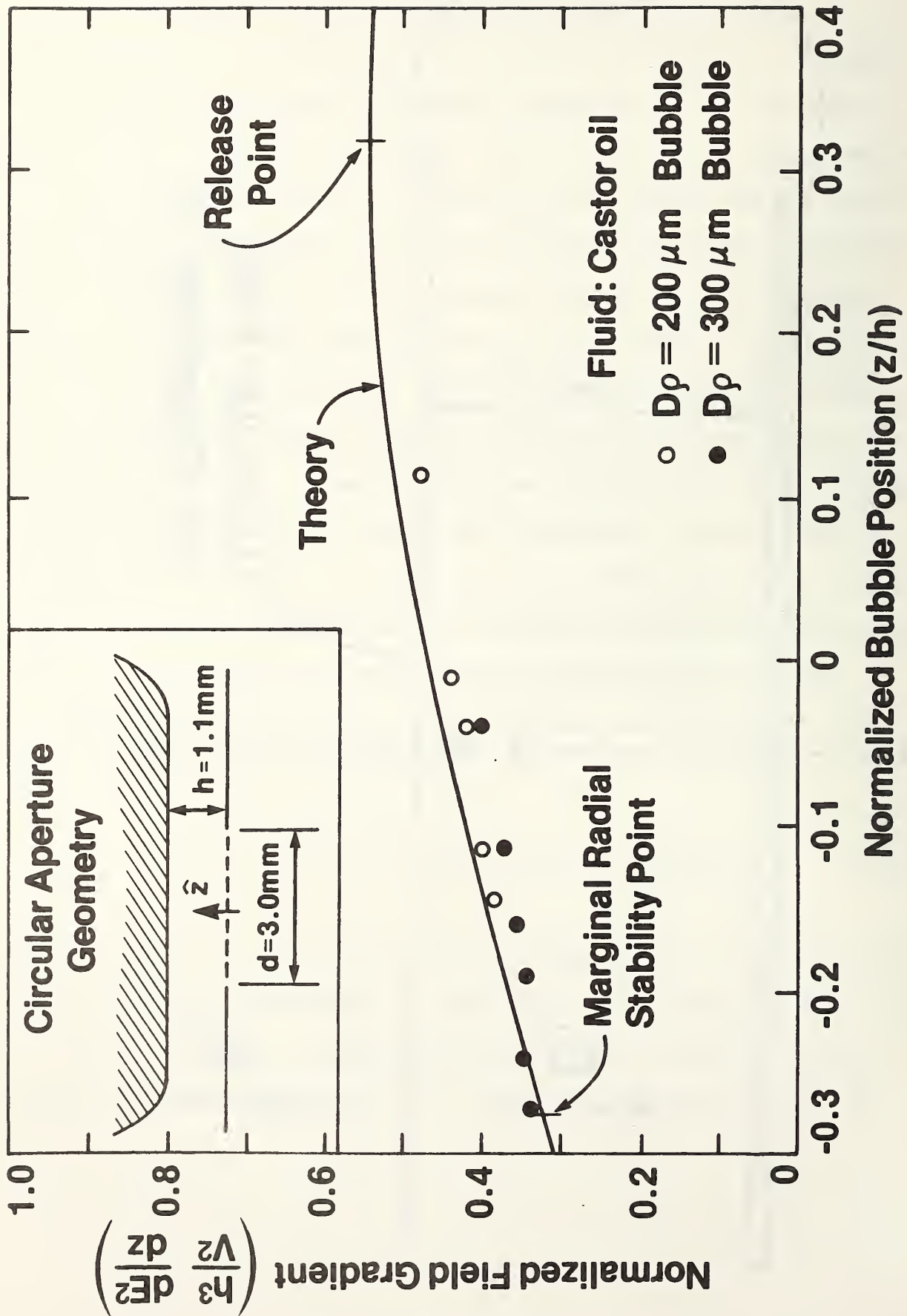
Figure 22. Normalized axial electric field gradient map for circular aperture geometry (d = 3.0 mm, air bubbles in castor oil).

The theory from Eq. 52 with $E_1 = 0$ is plotted to show the success of the
ideal electrostatic field solution in predicting device behavior.

4.4.5. Theoretical Consideration

Theoretical work has been devoted to establishment of criteria
for identifying the locus of stable equilibrium points in axisymmetric
cusped electric fields. This work is discussed thoroughly elsewhere[14]
and is merely summarized here. The field expansion of Holmes[15] is used to
provide expressions for the electric field components correct to second
order in small displacements of a levitated particle from some equilibrium
point ($r = 0$, $z = z_p$) on the axis. The expansions are:

$$E_z = V [\alpha_0 + \alpha_1 z' + \alpha_2 (z'^2 - \frac{r^2}{2})] , \qquad (53)$$

$$E_r = V [- \frac{\alpha_1}{2} r - \alpha_2 r z'] . \qquad (54)$$

where $z' = z - z_p$, V is the applied voltage and the coefficients
α_0, α_1, α_2 are functions of the equilibrium point

$$\alpha_n(z_p) = \frac{1}{Vn!} \frac{\partial^n E_z}{\partial z^n} \bigg|_{r=0, z=z_p} . \qquad (55)$$

Table 9. Defining Limits of Stable DEP Levitation Locus

UPPER LIMIT	release point: $z = z_r$ $$\left(\frac{\partial E_z}{\partial z}\right)^2_{0,z_r} + E_z \left(\frac{\partial^2 E_z}{\partial z^2}\right)_{0,z_r} = 0$$
LOWER LIMIT	marginal radial stability point: $z = z*$ $$\left(\frac{\partial E_z}{\partial z}\right)^2_{0,z*} - 2E_z \left(\frac{\partial^2 E_z}{\partial z^2}\right)_{0,z*} = 0$$ electrostatic field null: $z = z_h$ $$\left(E_z\right)_{0,z_n} = 0$$

The upper limit on the locus (at the high electric field end) is always
defined by the release point $z = z_r$, where $\partial^2 E_z^2/\partial z^2 = 0$. The lower point
can be either a point where the particle is marginally stable, that is
$\partial^2 E^2/\partial r^2 = 0$, or a field null, where $E^2 = 0$. As a particle approaches
a point of marginal stability it reaches a location $(r = 0, z = z)$ where
the particle drifts off to the side indicating that radial stabilization
is lost. If instead the particle approaches a field null, then the voltage

can be increased without bound (theoretically) and the particle will not move from the null. Examples of both kinds of behavior have been observed in the electrode geometries tested experimentally and the theoretical criteria of Table 9 have successfully predicted this behavior. The ring-plane geometry exhibits a field null. Particles are not lost radially, even for very high voltages. The circular aperture geometry (with $E_1 = 0$), exhibits radial instability which is predicted by the criterion in Table 9. For the geometry shown in the inset of Fig. 22, the theory predicts a marginal stability point at $z/h = -0.28$ at a voltage of $V = 1.34$ kV (rms), while the experimental observed results are $z/h = -0.27$ and $V \simeq 1.3$ kV (± 0.1).

4.5. Gas-Solid Interfaces

4.5.1. Introduction

Measurements have been performed to determine, using the Pockels[16] effect, surface electric fields at vacuum-solid and at gas-solid interfaces.

4.5.2. Vacuum Interfacial Field Measurements

Vacuum-solid interfacial fields have been measured using the Pockels effect in both KDP and $LiNbO_3$. The results obtained using KDP have been previously reported[17] and show that vacuum interfacial surface charging does occur. $LiNbO_3$ has also been used as the electro-optical sensing and insulating material because: (1) a higher surface hold-off field can be attained (70 kV/cm compared to 25 kV/cm for KDP); (2) it is less susceptible to surface tracking and changes due to flashover discharges ($LiNbO_3$ has a higher melting temperature than KDP); and (3) it is not water soluble and is, therefore, easier to clean and handle. The test cell is shown in Fig. 23.
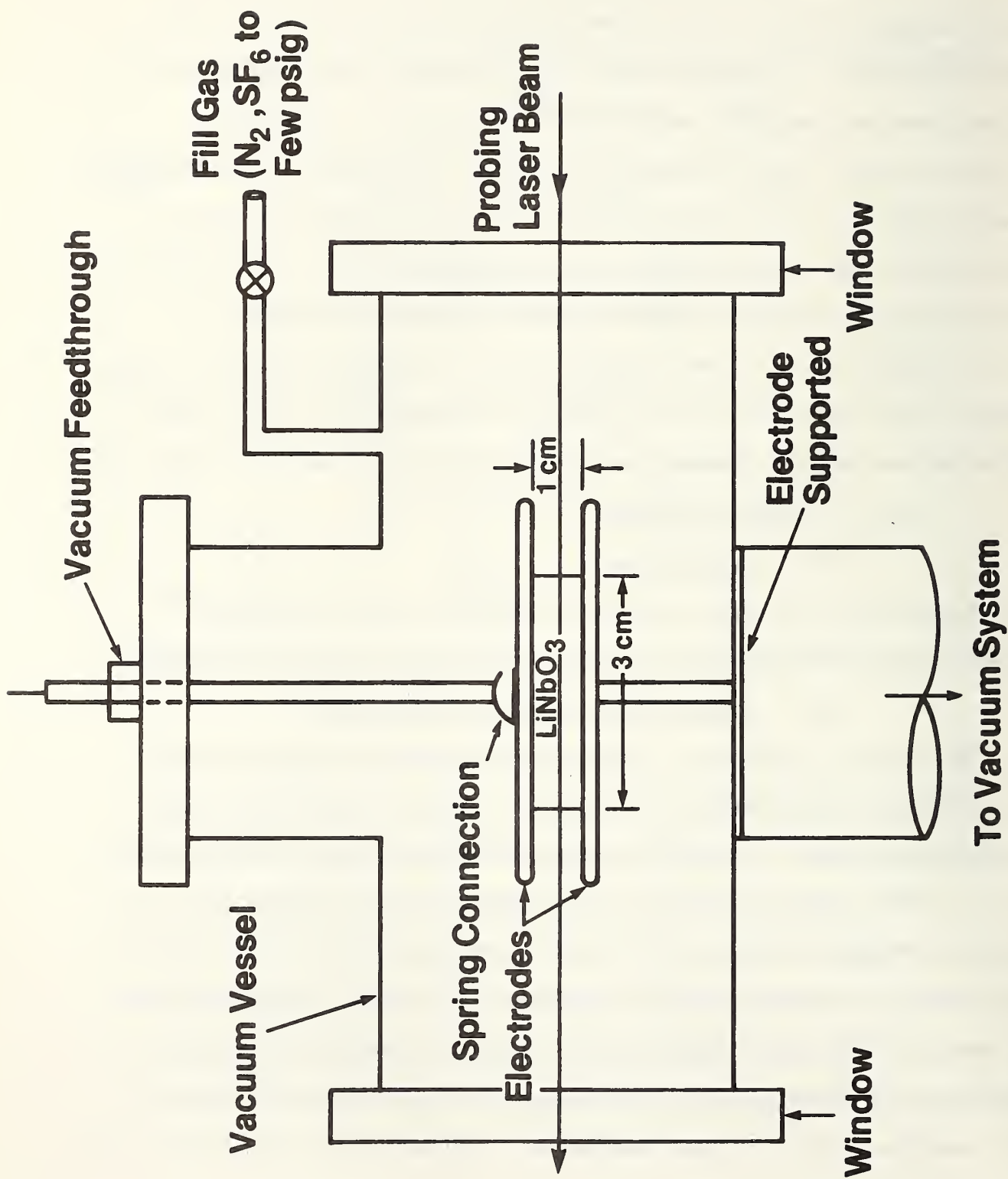
Figure 23. Vacuum and low pressure field measurement assembly.

Results obtained from vacuum-LiNbO$_3$ interfacial field measurements imply

that (1) the surface field varies linearly from anode to cathode; (2) surface

charge is removed by the addition of gas to the system; and (3) the tendency

for the insulator surface to maintain charge in vacuum decreases as the insulator

is conditioned.

The linear variation of the interelectrode field is such that the field is

enhanced at the cathode, relative to the average field value. This has been

observed for 60-Hz, dc, and pulsed excitations. Typical data illustrating

this is shown in Fig. 24. Electric field non-uniformity is indicated by the

bent and tilted fringes. The observed fringe deviation, Δz, at any position

(y,z) can be related to the field, $E(y,z)$ by

$$E(y,z) = 1.79 \times 10^5 \, \Delta z(y,z)/\delta z \quad , \tag{56}$$

where δz is the undeviated fringe spacing. Figure 24a shows the

interferometric data and Fig. 24b shows the computed field distribution

obtained from the interferogram. The field is seen to be enhanced at the

cathode and reduced at the anode by approximately the same amounts,

relative to the average field value. This will subsequently be shown

to be consistent with the fields associated with spatially uniform

positive surface charge. These charges are postulated to arise

from field emission from cathode protrusions and secondary electrons

cascading along the insulator surface.

The observed, spatially-varying field distribution remains after the

excitation has been removed. This is due to surface charges which remain

on the insulator surface. It has been observed that these surface charges
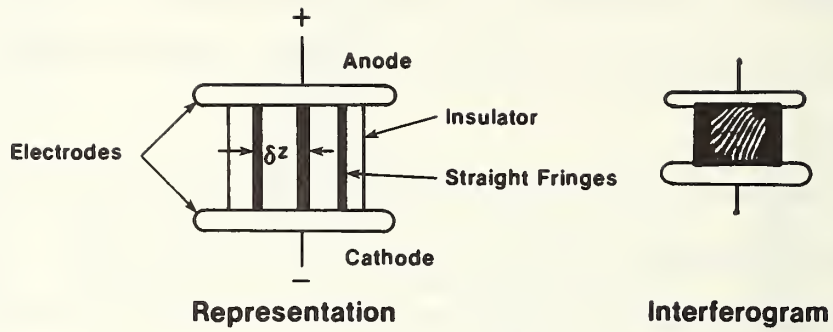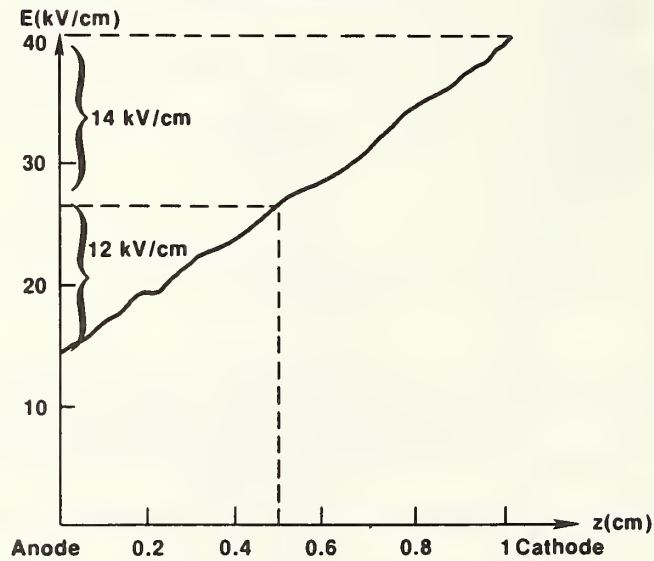
Figure 24. Interferogram and measured interfacial field variation for 25-kV peak, 60-Hz ac excitation.

can be removed by the addition of low pressure nitrogen. The displaced fringe behavior shown in Fig. 24a is indicative of charges residing on the insulator surface. The charged surface fringe behavior remains unchanged as N_2 gas is bled into the system until a pressure of 26.7 Pa is reached. The fringes are observed to relax almost instantaneously at this pressure, back to the fringe distribution which existed prior to excitation. From this behavior, it is inferred that the deposited surface charge is removed by the introduced gas when the gas pressure reaches a certain value. The charge removal process is accompanied by a glow discharge at the time of fringe relaxation.

It is postulated that the low pressure gas is ionized by the fields arising from the deposited surface charge. The ionized gas provides a discharge path and hence a removal mode for the surface charge. This observed result is significant because it shows that surface charge is deposited and resides on the insulator surface.

It should be noted that breakdown and charge removal can occur in a similar manner for a highly stressed vacuum interface where the gas is introduced by electron stimulated desorption from the insulator surface. This would be consistent with the flashover model postulated by Anderson and Brainard[18] which proposes that the vacuum gap breakdown is due to ionization of desorbed insulator surface gasses.

The tendency of the insulator surface to maintain charge has been observed to diminish as the insulator is conditioned by applying a near flashover value of voltage for an extended period of time. The magnitude of the surface charge has also been observed to be less after a conditioning period.

The reduced surface charge probably arises from the reduction, by microdischarges, of the number of electron emission sites on the cathode. It, however, appears that conditioning not only modifies the source of charging electrons but also reduces the insulator surface resistivity. It has been observed in this work, and the work of others, that the flashover voltage of conditioned insulators exceeds that of unconditioned insulators due to the removal of cathode electron-emission sites or a change in the secondary emission characteristics; further, reduced surface-charge retention time arising from a modification of the insulator's surface resistivity from conditioning has also been observed.

4.5.3. Low Gas Pressure Surface Electric Field Measurements

Measurements, obtained using KDP, have shown that no measurable, interfacial field nonuniformity occurs along KDP-gas interfaces in 1×10^5 Pa SF_6. This implies that negligible surface charge is deposited along KDP-gas interfaces for pressures up to 1×10^5 Pa.

Interferograms have also been obtained, using the test arrangement of Fig. 23, for $LiNbO_3$-N_2 and $LiNbO_3$-SF_6 interfacial field measurements for gas pressures of 1×10^5 Pa.

Interferograms obtained for $LiNbO_3$-N_2 (1×10^5 Pa) are shown in Fig. 25. A maximum peak field of 30 kV/cm was obtained before gap failure. The fringes shown in Fig. 25 remain straight and indicate no measurable surface charging. The breakdown was observed to occur, not
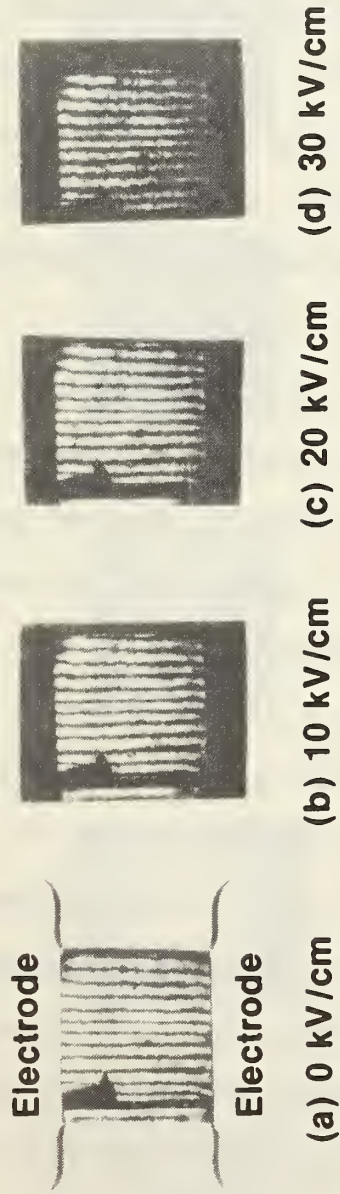
Figure 25. Field interferograms for $LiNbO_3-N_2$ interfaces and 60-Hz ac excitation.

Electrode

Electrode

(a) 0 kV/cm   (b) 10 kV/cm   (c) 20 kV/cm   (d) 30 kV/cm

along the insulator surface, but through the N_2 gas, approximately 1 cm away from the solid-N_2 interface. This observation is consistent with the low pressure data of Laghari and Qureshi.[19] They observed that the flashover path moved towards the solid-gas interface as the gas pressure was increased. Laghari and Qureshi observed that the spacer efficiency decreases from a value of unity at atmospheric pressure to approximately 0.7 as the pressure is increased to several atmospheres. He further observed that breakdown occurred along the spacer-gas interface at high pressures but through the gas, away from the insulator surface, at atmospheric pressure. This suggests that the surface, and perhaps surface charging, becomes important only at higher pressures.

Interferograms indicative of the $LiNbO_3$-SF_6 interfacial fields are shown in Fig. 26. Field values as high as 72 kV/cm were used and the gas was at atmospheric pressure. No flashover was observed even for these extreme field values. The fringes remain straight and indicate that no measurable $LiNbO_3$-SF_6 interfacial charging occurred.

The interfacial fields along a KDP-gas interface have been measured for pressures up to 4.1×10^5 Pa using the experimental arrangement of Fig. 23. Typical interferograms are shown in Fig. 27. The interferogram of 27a corresponds to no applied field. The interferogram of Fig. 27b was taken at the positive peak of a 60-kV/cm excitation. It should be noted that the image quality shown in Fig. 27 is lower than desired since a damaged KDP crystal is being used. Unfortunately this is the only remaining crystal. Careful analysis of the interferograms of 27a and b

Figure 26. Field interferograms for LiNbO$_3$-SF$_6$ interfaces and 60-Hz ac excitation.

Electrode

Electrode

(a) 5 kV/cm   (b) 10 kV/cm   (c) 20 kV/cm   (d) 35 kV/cm   (e) 72 kV/cm

(a) No field

(b) With field, 60 kV/cm
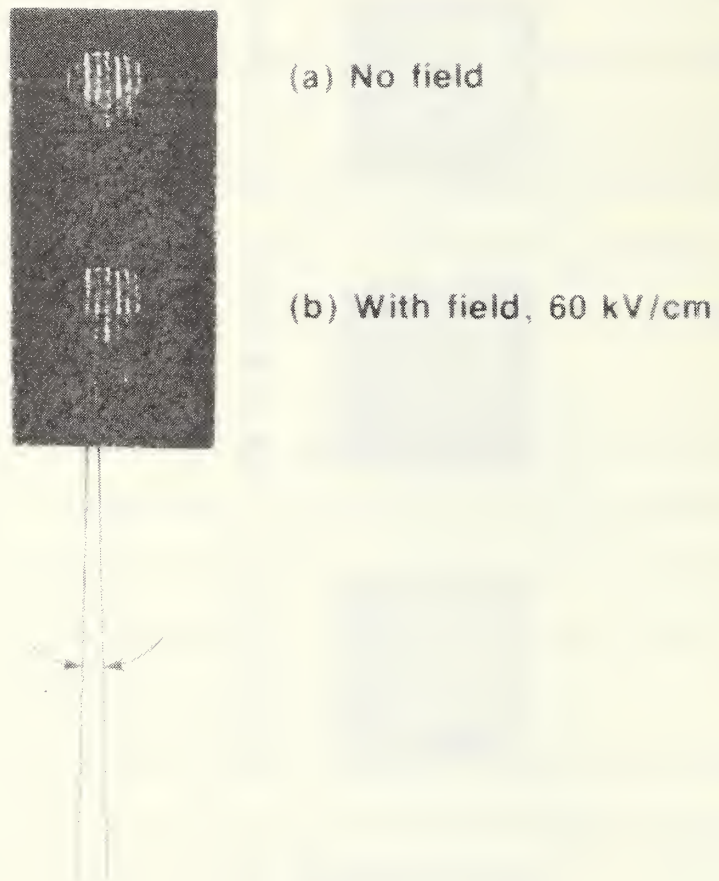
Figure 27. With a pressure of 4.14×10^6 Pa, the fringe pattern changes when a field is applied to a KDP-N_2 interface.

shows that the fringes of b are bent slightly with respect to the fringes
of a. This implies that a surface-charge-induced field nonuniformity is
present during the peak excitation. The deviation is clearly indicated
in Fig. 27 by the two lines tangent to the fringes in Figs. 27a and b. The
tangents are not parallel. This indicates that the fringes are not parallel.
The angle between the fringes is measured to be 3°.

The observed fringe shift is related to the electric field, for the
transverse Pockels effect, by

$$\frac{\Delta z}{\delta z} = \frac{N_o{}^3 r_{63}\ell}{2\lambda} E ,$$ (57)

where $N_o{}^3$ and r_{63} are known electro-optical constants, ℓ is the crystal
length, and λ is the probing laser wavelength. Solving Eq. 57 for the system
used shows that there is one fringe shift per 8 kV/cm. The data of Fig. 27
show that the fringes corresponding to excitation are deviated approximately
1 fringe, or 8 kV/cm for an applied field of 60 kV/cm. The fractional field
change from anode to cathode is, therefore, 8 kV/60 kV = 0.13. The
present data indicate a nonuniform electric field and hence surface charge.
It should, however, be noted that the data is presently judged
to be preliminary. Efforts are being made to improve the image quality
to facilitate more accurate fringe displacement measurements. It
is expected that surface charging will increase at higher electric field
values. Higher fields, however, cannot be obtained with the available
KDP due to track damage. The maximum field attainable without flashover
along the track damage is 60 kV. Higher field values will be employed in
upcoming measurements using more practical insulators and the Kerr effect
measurement technique.

5. SUMMARY

Among the significant technical outputs of this work are :

1. Analyses have been performed to determine the relationship between the measured field and the interfacial surface charge;

2. The electric field distribution in transformer oil has been measured using the electro-optic Kerr effect under both 60-Hz and impulse voltage waveforms using parallel-plate electrodes;

3. For a carefully prepared, paper-oil interface the breakdown voltage for breakdowns which occur at the interface is not necessarily lower than the voltage at which breakdowns occur away from the interface;

4. Under uniform field conditions in transformer oil, both anode and cathode streamers exist with the cathode streamer development a three-step process and anode streamer development a two-step process;

5. Dielectrophoretic levitation sensitivity has been analyzed and apparatus has been developed for the study of dielectrophoretic effects in selected systems;

6. A vacuum-solid interfacial field is non-uniform with the field enhanced at the cathode and reduced at the anode;

7. Conditioning of the vacuum-solid interface studied reduces both the surface charge and the surface charge retention;

8. No surface charging on the solid studied has been observed for N_2 or SF_6 at a pressure of 8.3 X 10^{-6} Pa.

6. ACKNOWLEDGMENTS

7. REFERENCES

1. H.P. Moser (privately published by EHV-Weidmann Lim., St. Johnsburg, VT, 1979), pp. 50-52.

2. See, For example, K. Wechsler, and M. Riccitiello, "Electric Breakdown of a Parallel Solid and Liquid Dielectric System," Trans. AIEE, Vol. 80, pp. 365-369 (1961).

3. E.A. Cherney, and J.D. Cross, "Electric Field Distortions at Solid-Liquid Dielectric Interfaces," IEEE Trans, Elec. Insul., Vol. EI-9, pp. 37-42 (1974).

4. E.C. Cassidy, R.E. Hebner, M. Zahn, and R.J. Sojka, "Kerr-Effect Studies of an Insulating Liquid Under Varied High Voltage Conditions," IEEE Trans. Elect. Insul., Vol, EI-9, pp. 43-56 (1974).

5. J.D. Cross, and R. Tobazeon, "Electric Field Distortions Produced by Solid Dielectric Spacers Separating Uniform Field Electrodes in Nitrobenzene," IEEE Trans. Elect. Insul., Vol. EI-8, pp. 25-29 (1973).

6. A.E. Cherney, and J.D. Cross, "Electrical Breakdown at Solid-Liquid Interfaces," IEEE Trans. Elect. Insul., Vol. EI-12, pp. 214-218 (1977).

7. F. Frey, and P. Atten, "Solid Spacer Influence on the Liquid Motion Induced by Unipolar Injection," J. Electrostatics, Vol. 5, pp.145-155 (1978).

8. D. F. Binns, "Breakdown Between Bare Electrodes in Transformer Oil," Proceedings of the Sixth International Conference on Conduction and Breakdown in Dielectric Liquids, Editions Frontieres, Dreux, France, pp. 111-116 (1978).

9. R. J. Taylor, "Effect of Permittivity Matching on the Flashover of Solid/Liquid Interfaces," Proc. IEE, Vol. 124, pp. 899-904 (1977).

10. J. K. Nelson, H. Sabuni, and P. B. McGrath, "Impulse Breakdown of Oil-Paper Insulation in the Vicinity of a Transformer Oil Duct Spacer," Proc. Third International Conference on Dielectric Materials, Measurements and Applications, IEE Conference Publication Number 177, pp. 14-17 (1979).

11. E. F. Kelley, and R. E. Hebner, "Measurement of Prebreakdown Electric Fields in Liquid Insulants," 1978 Annual Report: Conference on Electrical Insulation and Dielectric Phenomena (National Academy of Sciences, 1978), pp. 206-212.

12. G. A. Kallio, and T. B. Jones, "Dielectric Constant Measurements Using Dielectrophoretic Levitation," IEEE/IAS Conf., Toronto, 1978 (paper #IAS 78:4B).

13. A. B. El-Kareh, and J. C. C. El-Kareh, Electron beams, lenses, and optics, (Academic Press, New York, 1970) Section 3.8.

14. T.B. Jones, "Cusped Electrostatic Fields for Dielectrophoretic Levitation," submitted to publication J. Electrostatics.

15. L.M. Holmes, "Stability of Magnetic Levitation," J. Appl. Phys., Vol. 49, p. 3103 (1978).

16. J.A. Giordmaine, "Optics, Nonlinear," in Encyclopedia of Physics ed. by R.G. Lerner and G.L. Triggo, Reading, Ma.: Addison-Wesley, 1981.

17. J.E. Thompson, D. Hyslop, and T.S. Sudarshan, "Electro-Optical Measurement of Insulator Surface Preflashover Fields in Vacuum," 1979 Annual Report: Conference on Electrical Insulation and Dielectric Phenomena, (National Academy of Sciences, Washington, D.C.) pp. 334-344 (1979).

18. R.A. Anderson, and J.P. Brainard, "Surface-Flashover Model Based on Electron-Stimulated Desorption," 8th International Symposium on Discharges and Electrical Insulation in Vacuum, Albuquerque, NM (1978).

19. J.R. Laghari, and A.H. Qureshi, "Surface Flashover Voltages in SF_6-N_2 Mixtures Under Uniform and Non-Uniform DC Fields," 1979 Annual Report: Conference on Electrical Insulation and Dielectric Phenomena (National Academy of Sciences, Washington, D.C.) pp. 268-279 (1979).

8. PUBLICATIONS AND TALKS

During FY 80, the following were prepared and/or presented or published.

E. F. Kelley, and R. E. Hebner, "Time Evolution of the Electric Field Associated with Breakdown Phenomena in Liquids," 1979 Annual Report: Conference on Electrical Insulation and Dielectric Phenomena (National Academy of Sciences, Washington, D.C.) pp. 203-211, 1979.

J. E. Thompson, D. Hyslop, and T. S. Sudarshan, "Electro-Optical Measurement of Insulator Surface Preflashover Fields in Vacuum," 1979 Annual Report: Conference on Electrical Insulation and Dielectric Phenomena (National Academy of Sciences, Washington, D.C.) pp. 334-344, 1979.

D. E. Cooper, T. C. Cheng, K. S. Kim, K. Kantak, and J. Sletback, "Kerr Effect Measurements of Electric Fields in Crosslinked and Uncrosslinked Polyethylene," 1979 Annual Report: Conference on Electrical Insulation and Dielectric Phenomena (National Academy of Sciences, Washington, D.C.) p. 389, 1979.

R. E. Hebner, "Streamers in Liquids: Basic Phenomena and Practical Applications," invited talk at 14th Electrical/Electronics Insulation Conference, Boston, MA, 1979.

T. B. Jones, and J. J. McCarthy, "Electrode Geometries for Dielectrophoretic Levitation," Submitted to J. Electrostatics, 1980.

T. B. Jones, "Cusped Electrostatic Fields for Dielectrophoretic Levitation," submitted to J. Electrostatics, 1980.

E. F. Kelley, "Streamers in Liquids: Electric Field Distributions and Propagation Parameters," talk presented at the ASTM Symposium: Mechanism of Dielectric Breakdown in Liquids, San Francisco, CA, 1980.

E. F. Kelley, and R. E. Hebner, "Breakdown Between Bare Electrodes with an Oil-paper Interface," Nat. Bur. Stand., Washington, D.C. (U.S.) NBSIR 80-2071 (1980).

E. F. Kelley, and R. E. Hebner, "The electric field associated with prebreakdown phenomena in nitrobenzene," accepted by the Journal of Applied Physics, 1980.

E. F. Kelley, and R. E. Hebner, "Prebreakdown phenomena between sphere-sphere electrodes in transformer oil," accepted by Applied Physics Letters, 1980.

D. M. Hyslop, J. E. Thompson, and T. S. Sudarshan, "Electro-optical Measurements of Solid Insulator Surface Fields and Surface Charging in Vacuum," National Bureau of Standards Report GCR 80-203, 1980.

E. F. Kelley, and R. E. Hebner, "Electrical Breakdown in Composite Insulating Systems: Liquid-Solid Interface Parallel to the Field," accepted by IEEE Transactions on Electrical Insulation, 1980.

T.B. Jones and M.J. McCarthy, "Dielectric Measurements an Particles Using Dielectrophoretic Levitation," 1980 Annual Report: Conference on Electrical Insulation and Dielectric Phenomena (National Academy of Sciences, Washington D.C.) pp. 82-93, 1980.

U.S. DEPT. OF COMM. **BIBLIOGRAPHIC DATA SHEET** (See Instructions)	1. PUBLICATION OR REPORT NO. NBSIR 81-2275	2. Performing Organ. Report No.	3. Publication Date

4. TITLE AND SUBTITLE

1980 Annual Report: Optical Measurements for Interfacial Conduction and Breakdown

5. AUTHOR(S)

R.E. Hebner, E.F. Kelley, J.E. Thompson, T.S. Sudarshan, and T.B. Jones

6. PERFORMING ORGANIZATION (If joint or other than NBS, see Instructions) **NATIONAL BUREAU OF STANDARDS** **DEPARTMENT OF COMMERCE** **WASHINGTON, D.C. 20234**	7. Contract/Grant No. EA-88-01-6010 A057-EES
	8. Type of Report & Period Covered Annual 1980

9. SPONSORING ORGANIZATION NAME AND COMPLETE ADDRESS (Street, City, State, ZIP)

Office of Electric Energy Systems
Department of Energy
12th Street and Pennsylvania Avenue, N.W.
Washington, D.C. 20461

10. SUPPLEMENTARY NOTES

☐ Document describes a computer program; SF-185, FIPS Software Summary, is attached.

11. ABSTRACT (A 200-word or less factual summary of most significant information. If document includes a significant bibliography or literature survey, mention it here)

Techniques have been developed to measure the electric field distribution along an interface between insulating materials. Specifically, systems have been developed to measure the fields in transformer oil using the Kerr effect and to measure the surface charge at a gas-solid interface using the Pockels effect. Measurements are supplemented by calculations of the distortion produced by selected interfacial charge distributions. The relatively pure transformer oil used in these studies showed little space charge distortion of the electric field. There also was no statistically significant preference for breakdown in the vicinity of the interface. At vacuum-solid interfaces, however, interfacial breakdown was observed and surface charging was measured. As gas is introduced into the system, the surface charge is removed so that no effect of surface charging was detected at atmospheric pressure. At pressures above atmospheric, there is evidence that surface charging may again become important.

12. KEY WORDS (Six to twelve entries; alphabetical order; capitalize only proper names; and separate key words by semicolons)

dielectrics; electro-optics; gases; high voltage; insulation; interfaces; Kerr effect; liquids; Pockels effect; solids

13. AVAILABILITY	14. NO. OF PRINTED PAGES
☒ Unlimited ☐ For Official Distribution. Do Not Release to NTIS ☐ Order From Superintendent of Documents, U.S. Government Printing Office, Washington, D.C. 20402. ☒ Order From National Technical Information Service (NTIS), Springfield, VA. 22161	85
	15. Price $ 9.50